ROBUST ENSEMBLE KALMAN FILTERS AND LOCALIZATION FOR MULTIPLE STATE VARIABLES

A Dissertation

by

SOOJIN ROH

Submitted to the Office of Graduate and Professional Studies of
Texas A&M University
in partial fulfillment of the requirements for the degree of

DOCTOR OF PHILOSOPHY

Chair of Committee,	Mikyoung Jun
Co-Chair of Committee,	Marc G. Genton
Committee Members,	Bani K. Mallick
	Istvan Szunyogh
Head of Department,	Simon Sheather

August 2014

Major Subject: Statistics

ABSTRACT

Ensemble Kalman filters (EnKF) is a statistical technique used to estimate the state of a nonlinear spatio-temporal dynamical system. This dissertation consists of three parts. First, we develop a methodology to make EnKF robust, based on the employment of robust statistics. This methodology is necessary, since current EnKF algorithms tend to be sensitive to gross observation errors caused by technical or human errors during the data collection process, resulting in large biases or error variances. Second, we discuss the localization in the EnKF algorithms for simultaneous estimation of multiple state variables. The localization of the background-error covariance has proven to be an efficient method in reducing the sampling errors and compensating with the underestimation of the background error covariance terms. For a system of multiple state variables, the localization should be carefully applied in order to guarantee positive-definiteness of the matrices of the filtered background-error covariances. Rigorous localization methods for the case of multiple state variables, however, have rarely been considered in the literature. We introduce a number of localization filters that ensure that the background-error covariance matrix is positive-definite. Lastly, we extend the proposed robust method to both linear and nonlinear dynamical systems of multiple state variables.

To Kihun

ACKNOWLEDGEMENTS

I would like to thank my committee chair, Mikyoung Jun, and co-chair, Marc G. Genton, for their guidance on choosing a fascinating research path and their help throughout my doctoral study. Their support and encouragement allowed me to conduct my research continuously. Discussions with them have been particularly inspiring, as they always helped me understand and overcome complex problems. I would also like to express my gratitude toward my committee member, Istvan Szunyogh, for sharing his experience and knowledge about atmospheric sciences. I am thankful for his programming work, which became the foundation of my work, and all his endeavors to make me a better writer. I am grateful to my committee member, Bani Mallick, for reading and examining my dissertation.

I would like to thank my parents for letting me go on this challenging journey, since I understand that it requires a great courage to let their only daughter go so far, for supporting me with love throughout this study, and for all they have done for me in my entire life.

Lastly, I am especially thankful to my beloved husband, Kihun, for his unconditional trust in me and my ability to overcome any hardships that come into my way. It was the best of luck that I met you during my doctoral study.

TABLE OF CONTENTS

Page

LIST OF FIGURES

FIGURE Page

LIST OF TABLES

TABLE Page

1. INTRODUCTION

Data assimilation is a statistical process of estimating the state of a spatio-temporal dynamical system by combining numerical models with observations made on the system. In particular, it consists of a *forecast* step that forms a preliminary guess about the state of the system, typically completed by a deterministic model, and an *update* step that corrects this guess based on the data. The prior state estimator at a given time, obtained in the forecast step, is called a *background*, and the updated state estimator is called an *analysis*. The assimilation method is typically a sequential process, where data is updated to obtain an analysis and the analysis is used as a background for the next forecast step.

The Kalman filter (KF) scheme is an example of sequential processes, which provides a complete solution for the state estimation in the case of linear dynamics. It was first developed by Kalman (1960) and Kalman and Bucy (1961), and various filters have been derived from the Kalman filter. The Kalman filter can be interpreted as an optimal linear estimator under the assumption that the probability distribution of the background and observation errors is a multivariate Gaussian distribution with a known covariance matrix.

Although the Kalman filter has been successfully implemented for a wide range of applications and has provided the closed form of solution to the background and analysis in a linear situation, it poses difficulties in nonlinear dynamics. The ensemble Kalman filter (EnKF) was originally introduced by Evensen (1994) based on the Kalman filter schemes to solve such problems as in atmospheric sciences, where the dynamical models are represented as the complicated nonlinear equations. The general idea of the ensemble-based Kalman filter is to use a sample of the state of

the system for discrete approximation to the continuous and often high-dimensional distribution of the state. This sample is called an *ensemble*. Each ensemble member is propagated forward in time using the model giving a new ensemble for approximating the forecast distribution, and is updated based on the data.

Although EnKF has long been considered for atmospheric data assimilation and has been developed by many researches (e.g. Houtekamer and Mitchell 1998; Anderson 2001; Whitaker and Hamill 2002), two important problems have still been around. First, the EnKF is so susceptible to observational outliers that they can degrade the precision of the state estimation. Second, there has not been full investigation of statistically valid methods used to make up for the loss due to the small sample size of the EnKF with a system of multiple state variables. While reducing the sampling error, a statistically invalid method can cause another issue which is a rank deficiency problem. The goal of this study consists of three parts: first, to develop a method to make EnKF robust to outliers; second, to introduce statistically valid methods to compensate for the sampling errors resulting from the small sample size in the multivariate system; and lastly, to extend the developed robust method to the case of multiple state variables in both linear and nonlinear system.

To this end, first, we review the formulations of EnKF algorithm and examine related problems and possible solutions.

1.1 Formulations of Ensemble Kalman Filter

We let $\mathbf{x}_t \in \mathbb{R}^n$ be a finite-dimensional representation of the state of the atmosphere at time t, and

$$\mathbf{x}_t = \mathcal{M}(\mathbf{x}_{t-1}) \tag{1.1}$$

a model for the evolution of the state between discrete times with a fixed interval. For the sake of simplicity, we assume that observations of the state are taken at discrete

times, for which the model solution is available, and that the functional relationship between the state and the vector of observations, $\mathbf{y}_t \in \mathbb{R}^p$, at time t is

$$\mathbf{y}_t = \mathbf{H}_t \mathbf{x}_t + \boldsymbol{\epsilon}_t. \tag{1.2}$$

Here, $\mathbf{H}_t \in \mathbb{R}^{p \times n}$ is the observation operator and the random variable, $\boldsymbol{\epsilon}_t \in \mathbb{R}^p$, is the observation error, which is assumed to be a zero-mean (Gaussian) process with a known covariance matrix, $\mathbf{R}_t$. The Kalman filter provides an estimate of the state, $\mathbf{x}_t$, based on the observations taken at the past and the present observation times and on the assumed knowledge (model) of the dynamics.

An EnKF algorithm assumes the availability of an M-member ensemble (sample), $\{\mathbf{x}_t^{b(k)} : k = 1, \ldots, M\}$, of a priori state estimates (backgrounds) with random sample errors available at time t. This ensemble is called the background ensemble. The mean of the background ensemble, $\bar{\mathbf{x}}_t^b$, which is called the background, is our best estimate of the state $\mathbf{x}_t$ before the assimilation of the observations taken at time t. The analysis step of an EnKF generates an analysis ensemble, $\{\mathbf{x}_t^{a(k)} : k = 1, \ldots, M\}$, such that its mean, $\bar{\mathbf{x}}_t^a$, called the analysis, satisfies

$$\bar{\mathbf{x}}_t^a = \bar{\mathbf{x}}_t^b + \mathbf{K}_t(\mathbf{y}_t - \mathbf{H}_t \bar{\mathbf{x}}_t^b), \tag{1.3}$$

while the ensemble-based estimate of the analysis error covariance matrix, $\mathbf{P}_t^a \in \mathbb{R}^{n \times n}$, which is defined by the sample mean covariance matrix for the ensemble, satisfies either

$$\mathbf{P}_t^a = (\mathbf{I} - \mathbf{K}_t \mathbf{H}_t)\mathbf{P}_t^b, \tag{1.4}$$

without the perturbed observations or

$$\mathbf{P}_t^a = (\mathbf{I} - \mathbf{K}_t\mathbf{H}_t)\mathbf{P}_t^b + O(M^{-1/2}) \tag{1.5}$$

with the perturbed observations. In Eqs. (1.3), (1.4), and (1.5), the Kalman gain matrix, $\mathbf{K}_t \in \mathbb{R}^{n\times p}$, is given by

$$\mathbf{K}_t = \mathbf{P}_t^b\mathbf{H}_t^T(\mathbf{H}_t\mathbf{P}_t^b\mathbf{H}_t^T + \mathbf{R}_t)^{-1}, \tag{1.6}$$

and the ensemble-based estimate of the background error covariance matrix, $\mathbf{P}_t^b \in \mathbb{R}^{n\times n}$, is provided by the sample covariance matrix for the background ensemble. In our numerical experiments, we use the method of perturbed observations (Houtekamer and Mitchell 1998; Burgers et al. 1998) to obtain the analysis ensemble. In this technique, $\mathbf{P}_t^a$ satisfies Eq. (1.5). The analysis process at time t is completed by the forecast step of the EnKF, in which the model dynamics is applied to each member of the analysis ensemble to obtain the members of the background ensemble for the next observation time, $t + 1$.

1.2 Issues for Ensemble Kalman Filter

This section reports two important issues in implementing the EnKF schemes. First, current EnKF algorithms are not robust to gross observation errors (Schlee et al. 1967; Ruckdeschel 2010). Second, the univariate localization methods can cause the rank-deficiency problem when it is applied directly to the EnKF algorithms for multiple state variables. In the following, we consider each of these issues in turn.

1.2.1 Sensitivity to observational outliers

In Eq. (1.3), the components of the vector of differences, $\mathbf{y}_t - \mathbf{H}_t \bar{\mathbf{x}}_t{}^b$, between the observations and their predicted values are called *innovations*. Each innovation describes the discrepancy between an observation and its predicted value. In addition, the components of the change in the state estimate, $\bar{\mathbf{x}}_t^a - \bar{\mathbf{x}}_t^b$, due to the assimilation of the observations included in $\mathbf{y}_t$, are called *analysis increments*. The role of the Kalman gain matrix, $\mathbf{K}_t$, is to map the innovations into analysis increments. According to Eq. (3.2), the Kalman gain accounts for the observation errors based on the prescribed error statistics included in $\mathbf{R}_t$. It thus has no information about the errors in a particular observation or the magnitude of a particular innovation. Since the analysis increments are unbounded functions of the innovations, a large innovation due to a gross (outlier) observation error can cause a large degradation in the accuracy of the state estimate.

1.2.2 Localization of multivariate ensemble covariance

In the EnKF algorithms, small sample size can cause sampling errors and underestimation of the background ensemble covariances, $\mathbf{P}^b$ (Houtekamer and Mitchell 1998; Whitaker and Hamill 2002). The localization of background ensemble covariance is often used to solve this problem in practice and to increase the accuracy of the analysis. In atmospheric data assimilation, the localization is usually achieved by applying a distance-dependent correlation filter function to the ensemble covariances (e.g.Houtekamer and Mitchell 1998; Hamill et al. 2001; Anderson 2001; Ott et al. 2004; Buehner and Charron 2007). The localization is obtained by Schur (elementwise) product of the background ensemble covariance from the ensemble and a localization matrix given from a compactly supported correlation function. Gaspari and Cohn (1999) introduced the convolution theorem in order to construct the

polynomial localization functions with a compact support. They are the most popular used correlation function in the atmospheric data assimilation. Askey (1973) and Wendland (1995) introduced compactly supported radial basis functions on the Euclidean space $\mathbb{R}^3$, and Gneiting (1999, 2002) discussed radial positive-definite functions studied by Askey (1973).

Until recently, the efforts to develop the localization methods have been concentrated to the EnKF for the systems of a single state variable. Statistically valid localization methods for EnKF with multiple state variables are rarely considered in the literature, while the currently used localization techniques are proved to be mathematically rigorous in the system of only one state variable. Applying the univariate localization directly to the system of multiple state variables can result in a localization matrix which has its eigenvalue of zero and is not positive-definite. In the case of multiple state variables, the ensemble covariance estimate should be carefully localized in order to guarantee its positive-definiteness.

1.3 Overview of Dissertation

The main goal of this dissertation is to make the ensemble Kalman filter robust to outliers in observations, and to propose statistically valid localization methods for the EnKF algorithms with multiple state variables. Chapter 2 proposes the robust ensemble Kalman filter by using the Huber function, the well-known function in robust statistics. Chapter 3 introduces multivariate localization methods to ensure the positive-definiteness of the multivariate ensemble-based estimate of the background error covariance by adjusting the cross-covariance terms. Since there is an increasing need to simultaneously estimate the several state variables, and the robust approach in Chapter 2 focuses on the univariate systems, Chapter 4 applies the proposed robust method and explore its working to both linear and nonlinear dynamics of multiple

state variables. This chapter also briefly reviews the Kalman filter algorithms in a linear situation. Finally, Chapter 5 summarizes the main results of this dissertation.

2. ROBUST ENSEMBLE KALMAN FILTER*

In this chapter, we investigate the effect of observational outliers on the ensemble Kalman filter, and consider two types of gross observational errors; additive outliers and innovation outliers. We introduce a method to make EnKF robust to gross observation errors. Using both a one-dimensional linear system and the 40-variable Lorenz model, the performance of the proposed robust ensemble Kalman filter (REnKF) was tested. It was found that this new approach greatly improves the performance of the ensemble Kalman filter in the presence of gross observation errors and leads to only a modest loss of accuracy with clean, outlier-free, observations.

2.1 Introduction

In data assimilation, the process of detecting and accounting for observation errors that are statistical outliers is called *quality control* (QC; e.g., Daley 1991). An operational numerical weather prediction system may employ multiple layers of QC. For instance, observations with implausible values are usually rejected even before they enter the data assimilation process. We refer to the algorithms used for such rejection decisions as *off-line QC* algorithms. The fact that an observation passes the off-line QC procedures does not guarantee that it is not a statistical outlier, however. For instance, an error in a highly accurate observation can be a statistical outlier when the error has a large representativeness error component. Such errors have to be dealt with by the data assimilation algorithm. We refer to the QC procedures that are part of the data assimilation algorithms as *online QC* algorithms.

* Most of this chapter is reprinted from Roh et al. (2013) "Observation quality control with a robust ensemble Kalman filter," Monthly Weather Review, 141, 4414-4428.

Online QC algorithms detect observation errors that are statistical outliers by examining the difference between the observation and the prediction of the observation by the background. This difference is called the innovation. For instance, a simple online QC can be implemented by rejecting the observations for which the absolute value of the innovation is larger than a prescribed threshold. Another approach, which is more desirable from a theoretical point of view, is to employ robust statistics in the formulation of the state-update step of the data assimilation scheme (e.g., Huber 1981; Hampel 1986; Maronna et al. 2006). In particular, the presumed probability distribution of the observation errors can be modified such that the update step can anticipate errors that would be considered statistical outliers if the observation errors were strictly Gaussian. The practical challenge posed by this approach is to find a modification of the prescribed probability distribution function, which leads to a data assimilation algorithm that can be implemented in practice.

An operational online QC algorithm using robust observation error statistics (Anderson and Järvinen 1999) was first introduced by the European Center for Medium Range Weather Forecasts (ECMWF). The general idea of this approach was to define the probability distribution of the observation errors as the sum of two probability distributions: a normal distribution representing the "normal" observation errors, and another distribution representing the "gross" observation errors. This approach was originally proposed as an off-line QC procedure by Ingleby and Lorenc (1993), but the variational framework made its integration into the data assimilation scheme possible. The formulation of the algorithm by Anderson and Järvinen (1999) became known as Variational QC (Var-QC). In the latest operational version of Var-QC, called the Huber norm QC (Tavolato and Isaksen, 2010), the probability of medium and large observation errors decreases linearly making it faster than a Gaussian distribution, but slower than a uniform distribution.

A wide variety of robust filtering schemes has been proposed in the mathematical statistics literature in the past decades. In particular, Meinhold and Singpurwalla (1989) replaced the normality assumption by fat-tailed distributions such as the t distribution, whereas Naveau et al. (2005) considered a skewed version of the nomal distribution. West (1981, 1983, 1984) suggested a method for robust sequential approximate Bayesian estimation. Fahrmeir and Kaufmann (1991) and Fahrmeir and Kunstler (1999) offered posterior mode estimation and penalized likelihood smoothing in robust state space models. Kassam and Poor (1985) discussed the minimax approach for the design of robust linear filters for signal processing. Schick and Mitter (1994) derived a first-order approximation for the conditional prior distribution of the state. Ershov and Liptser (1978), Stockinger and Dutter (1987), Martin and Raftery (1987), Birmiwal and Shen (1993), and Birmiwal and Papantoni-Kazakos (1994) also proposed robust filtering schemes that were resistant to outliers.

Recently, Ruckdeschel (2010) proposed a robust Kalman filter in the setting of time-discrete linear Euclidean state-space models with extension to hidden Markov models, which is optimal in the sense of minimax mean squared errors. He used the Huberization method, but investigated its performance only on a one-dimensional linear system. Luo and Hoteit (2011) employed the H_∞ filter to make ensemble Kalman filters (EnKF) robust to gross background errors. The H_∞ filter minimizes the maximum of a cost function different from the minimum variance used in the Kalman filter. They demonstrated their approach on both a one-dimensional linear and a multidimensional nonlinear model. Calvet et al. (2012) introduced an impact function that quantified the sensitivity of the state distribution and proposed a filter with a bounded impact function.

EnKFs have been successfully implemented in highly complex operational prediction models in atmospheric and oceanic sciences. They are Monte Carlo approxima-

tions of the traditional Kalman filter (Kalman 1960) and use ensembles of forecasts to estimate the mean and the covariance of the presumed normal distribution of the background. Similar to KF, EnKFs are not robust to gross errors in the estimate of the background mean or the observation (e.g., Schlee et al. 1967). The main goal of this chapter is to design an EnKF scheme that is robust to observation errors that are statistical outliers. Harlim and Hunt (2007) and Luo and Hoteit (2011) made EnKF robust to unexpectedly large background errors. Here, we propose to make EnKF robust to gross observation errors by Huberization, a procedure that can be implemented on any EnKF scheme.

The rest of the chapter is organized as follows. Section 2.2 first illustrates the effects of gross observation errors on the performance of EnKF; then, it describes our proposed approach to cope with such errors. Section 2.3 demonstrates the effectiveness of our approach for a one-dimensional linear system, while Section 2.4 shows the results for the 40-variable Lorenz model.

2.2 Robust Ensemble Kalman Filter

In this section we examine the effect of observation outliers on the ensemble Kalman filter and two types of observation outliers, and discuss how to make the EnKF robust.

2.2.1 The effects of observation outliers

We consider two common types of observation outliers: additive outliers (AO) and innovations outliers (IO). (Fox 1972; Genton 2003; Genton and Lucas 2003, 2005). In an AO model, we observe

$$\mathbf{y}_t = \mathbf{H}\mathbf{x}_t + \boldsymbol{\xi}_t + \boldsymbol{\epsilon}_t, \tag{2.1}$$

where $\boldsymbol{\xi}_t \in \mathbb{R}^p$ is a vector of unknown outlying values. It is assumed that only a few components of $\boldsymbol{\xi}_t$ are different from zero. In an IO model, the observation error is assumed to be a contaminated multivariate Gaussian distribution,

$$\boldsymbol{\epsilon}_t \sim (1-\alpha)N_p(\mathbf{0}, \mathbf{R}_t) + \alpha N_p(\mathbf{0}, k_t \cdot \mathbf{R}_t), \tag{2.2}$$

where $0 < \alpha < 1$, $k_t = \text{diag}(k_{t1}, k_{t2}, \ldots, k_{tp})$, and $k_{ti} > 1$ for some $1 \leq i \leq p$. Here, N_p denotes the p-variate Gaussian distribution. For the innovations outlier models, the observation errors have a zero mean and a probability $1-\alpha$ of coming from a normal distribution with covariance matrix $\mathbf{R}_t$, and a (usually small) probability α of coming from a normal distribution with higher variances, $k_t \cdot \mathbf{R}_t$. The value of k_t is assumed to be unknown. The additive outlier model corresponds to a situation where some of the observations are affected by a strong observation bias, whereas the innovations outlier model corresponds to a situation where there is an $100 \times \alpha$ percent chance that the observation error variance is larger than the prescribed value given by $\mathbf{R}_t$.

We illustrate the effects of the type of outlier on EnKF analyses with the help of a one-dimensional linear system:

$$x_t = x_{t-1} + e_t, \tag{2.3}$$

and the observation equation:

$$y_t = x_t + \epsilon_t, \tag{2.4}$$

where e_t and ϵ_t are zero-mean Gaussian processes with unit variance. The results shown in Fig. 2.1 were obtained by using the traditional EnKF algorithm to obtain

the analysis ensemble that satisfies Eqs. (1.3) and (1.5) for Eqs. (2.3) and (2.4). We assimilate observations at every time step. The outliers occur at the times where the errors are marked by open circles. The top panel shows the results for the AO model, with $\xi_t = 5$ for the outliers, while the bottom panel shows the results for the IO model, with $\alpha = 0.2$ and $k_t = 25$ for the outliers. The accuracy of the state estimates are clearly degraded at the time steps where the outliers are present in either outlier model.

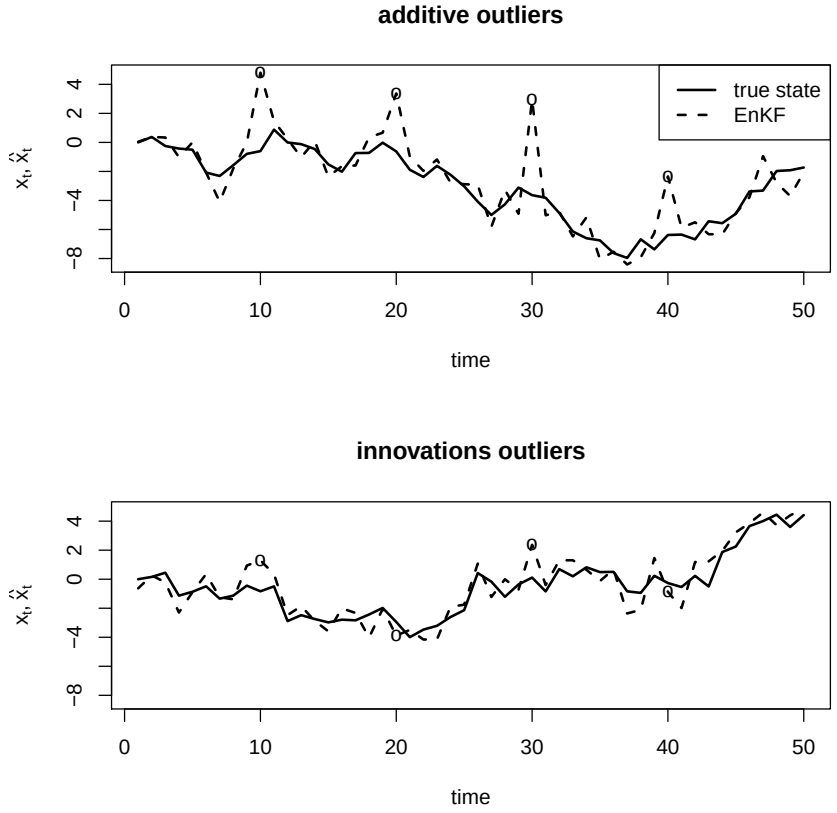

Figure 2.1: Plot of the (solid line) true states and (dashed line) the traditional ensemble Kalman filter as a function of time t for a one-dimensional linear system with (top) additive outliers $\xi_t = 5$ and (bottom) innovations outliers with $\alpha = 0.2$ and $k_t = 25$. The occurrences of outliers are marked with open circles.

2.2.2 A robust ensemble Kalman filter

The detrimental effect of the outliers on the EnKF state estimate can be reduced by decreasing the magnitude of those components of the innovation vector that have unusually large absolute values. This can be done by defining an upper bound for the allowable absolute value of the innovations. When the magnitude of an innovation is found to be larger than the prescribed upper bound, the magnitude of the innovation can be clipped at the upper bound. To be precise, the innovation δy is left unchanged if $-c < \delta y < c$ for some $c > 0$ and clipped at $-c$ if $\delta y < -c$ and at c if $\delta y > c$. This componentwise clipping of the innovation is called *Huberization*, and the tunable parameter, c, is called the *clipping height*.

The *Huberized analysis*, $\hat{\mathbf{x}}^a$, can be written as

$$\hat{\mathbf{x}}_t^a = \bar{\mathbf{x}}_t^b + \mathbf{K}_t G_{\mathbf{c}}(\mathbf{y}_t - \mathbf{H}_t \bar{\mathbf{x}}_t^b), \tag{2.5}$$

where for any $\mathbf{c} \in \mathbb{R}_+^p$ and $\mathbf{u} \in \mathbb{R}^p$, the *Huber* function, $G_{\mathbf{c}}(\mathbf{u})$, is defined by ($i = 1, \ldots, p$)

$$\{G_{\mathbf{c}}(\mathbf{u})\}_i = \begin{cases} u_i, & \text{if } |u_i| < c_i, \\ c_i, & \text{if } u_i \geq c_i, \\ -c_i, & \text{if } u_i \leq -c_i. \end{cases} \tag{2.6}$$

Here, c_i and u_i are the i-th elements of $\mathbf{c}$ and $\mathbf{u}$, respectively. The observation is clipped componentwisely by the clipping height of the same dimension. When Huberization achieves its goal of reducing the contamination of the prescribed distribution of the observation errors, the observation error covariance matrix, $\mathbf{R}_t$, provides a better representation of the observation error covariance. Hence, we do not modify any entries of $\mathbf{R}_t$.

A simple alternative to Huberization for handling observation error outliers is to discard the suspect observations from the data assimilation process. In fact, this is the online QC approach that has been employed by EnKF algorithms in weather prediction models (e.g., Szunyogh et al. 2008). In the simple numerical examples given here, we discard the observation if $|\delta y| > c$ for a prescribed c. In these applications, the prescribed smallest magnitude of the innovation that triggers a rejection of the observation depends on the magnitude of the ensemble-based estimate of the background error variance at the observation location (the related entry of $\mathbf{H}_t\mathbf{P}_t^b\mathbf{H}_t^T$) and/or the variance of the observation error (the related diagonal element of $\mathbf{R}_t$). Because this approach is based on discarding the observation rather than reducing the contamination from the observation error, the entries of $\mathbf{R}_t$ that are related to the discarded observation must also be removed.

2.2.3 Choosing parameter $\mathbf{c}$

The tunable parameter of both strategies to handle the outlier observation errors, which were described in Section 2.2.2, is the p-dimensional vector $\mathbf{c} \in \mathbb{R}^p$. An ideal choice for $\mathbf{c}$ would remove the contamination from the observation error or lead to rejection of the observation without making any change in the state estimates of clean, outlier-free, observations. While such an ideal choice for $\mathbf{c}$ usually does not exist, we can define a measure of our tolerance for degradation in the accuracy of the state estimates for clean observations.

One measure of tolerance can be defined by introducing the notion of *relative efficiency*. The relative efficiency of two algorithms to estimate the state is defined by the ratio of the variance of the error in the two estimates they provide. The

relative efficiency of EnKF with and without online QC,

$$\delta = \frac{\mathrm{E}|\mathbf{x}_t - \bar{\mathbf{x}}_t^a|_{id}^2}{\mathrm{E}|\mathbf{x}_t - \hat{\mathbf{x}}_t^a|_{id}^2}, \tag{2.7}$$

falls into the interval $\delta \in (0, 1]$. Here, $|\cdot|$ denotes the Euclidean norm and the subscript *id* indicates that the norm is to be computed for clean, outlier-free, observations. If no quality control were applied (the components of $\mathbf{c}$ were set to infinity), then the relative efficiency would be $\delta = 1$. Equivalently, achieving a perfect relative efficiency, $\delta = 1$, would require choosing $\mathbf{c} = \infty$. The lower the value of δ we accept, the lower the values we can choose for the components of $\mathbf{c}$. A common choice for the relative efficiency is $\delta = 0.95$ (e.g., Huber 1981).

In order to use the relative efficiency as a criterion for the selection of $\mathbf{c}$, we have to find a practical approach to computing the components of $\mathbf{c}$ for a given value of δ. In Kalman filtering, the variance of the analysis error is usually estimated by the trace of $\mathbf{P}_t^a$ given by Eq. (1.4). While this approach would provide a simple formula for the numerator in Eq. (2.7), the denominator could not be written with the help of Eq. (1.4), because $G_{\mathbf{c}}(\mathbf{u})$ is a nonlinear function of the innovation. It cannot thus be absorbed into the Kalman gain matrix. Hence, after dropping the subscript t that denotes the time, the only alternative left is to substitute $\bar{\mathbf{x}}^a$ from Eq. (1.3) and $\hat{\mathbf{x}}^a$ from Eq. (2.5) into Eq. (2.7), which yields

$$\delta = \frac{\mathrm{E}|\mathbf{x} - \bar{\mathbf{x}}^b - \mathbf{K}(\mathbf{y} - \mathbf{H}\bar{\mathbf{x}}^b)|_{id}^2}{\mathrm{E}|\mathbf{x} - \bar{\mathbf{x}}^b - \mathbf{K}G_{\mathbf{c}}(\mathbf{y} - \mathbf{H}\bar{\mathbf{x}}^b)|_{id}^2} = \frac{\mathrm{E}|\left(\mathbf{I} - \mathbf{K}\mathbf{H}\right)\left(\mathbf{x} - \bar{\mathbf{x}}^b\right) + \boldsymbol{\epsilon}|_{id}^2}{\mathrm{E}|\left(\mathbf{x} - \bar{\mathbf{x}}^b\right) - \mathbf{K}G_{\mathbf{c}}\left[\mathbf{H}\left(\mathbf{x} - \bar{\mathbf{x}}^b\right) + \boldsymbol{\epsilon}\right]|_{id}^2}. \tag{2.8}$$

The second equality comes from the observation equation (1.2).

The i-th component, c_i, of the clipping height, $\mathbf{c}$, is obtained by using

$$\mathrm{E}|\mathbf{x} - \bar{\mathbf{x}}^a|_{id}^2 = \mathrm{E}|\mathbf{x} - \bar{\mathbf{x}}^b - [\mathbf{K}]_i(\mathbf{y} - \mathbf{H}\bar{\mathbf{x}}^b)_i|_{id}^2, \tag{2.9}$$

for the computation of the numerator and

$$\mathrm{E}|(\mathbf{x} - \hat{\mathbf{x}}^a)|_{id}^2 = \mathrm{E}|\mathbf{x} - \bar{\mathbf{x}}^b - [\mathbf{K}]_i G_{\mathbf{c}_i}\{(\mathbf{y} - \mathbf{H}\bar{\mathbf{x}}^b)_i\}|_{id}^2, \tag{2.10}$$

for the computation of the denominator. In the above, $[\mathbf{K}]_i$ is the ith column of the Kalman gain matrix, $\mathbf{y} - \mathbf{H}\bar{\mathbf{x}}^b = \mathbf{H}(\mathbf{x} - \bar{\mathbf{x}}^b) + \boldsymbol{\epsilon}$, $\mathbf{x} - \bar{\mathbf{x}}^b \sim N_n(\mathbf{0}, \mathbf{P}^b)$, and $\boldsymbol{\epsilon} \sim N_p(\mathbf{0}, \mathbf{R})$. In Eqs. (2.9) and (2.10), the means are then computed using a Monte Carlo approach, sampling from these Gaussian distributions. The c_i used to clip the i-th innovation is chosen as if the analysis process consisted of assimilating the i-th observation only. The selected clipping heights vary according to whether we Huberize the observations to $\mathbf{c}$ or make them to $\mathbf{0}$. There is a precedent for this criterion of selecting a clipping height for robust Kalman filters (Ruckdeschel, 2010). In Ruckdeschel (2010), however, a one-dimensional clipping height is selected to clip the norm of the multidimensional observations for the multidimensional case. When outliers occur at few variables, the norm may not be changed much by these few outliers and therefore the outliers may not be clipped. The variables where the outliers do not occur should be evenly clipped once the one-dimensional clipping height is smaller than the norm. A multidimensional clipping height that we propose clips the elements that are considered to have outliers.

Another criterion is to select c_i such that

$$(1 - r)\mathrm{E}(|(\mathbf{y} - \mathbf{H}\bar{\mathbf{x}}^b)_i|_{id} - c_i)_+ = rc_i,$$

for a given radius $r \in (0,1)$. Here, $(x)_+ = |x| \cdot \max\{x/|x|, 0\}$. The radius r is a proportion of the amount of clipping in the innovation. The clipping heights are the same for either type of clipping because this criterion does not depend on how we clip innovations. A smaller radius provides a larger clipping height and fewer clipping outliers. This radius criterion has been used to select a clipping height in the robust Kalman filter scheme (Ruckdeschel, 2010).

The important issues in selecting the clipping height, $\mathbf{c}$, are the computational complexity of the sample covariance matrices. First, a small ensemble size may produce inaccurate estimates of the covariance matrices (Whitaker and Hamill 2002). Another is that doing the Monte Carlo integration method to choose the clipping height, $\mathbf{c}$, for all time steps is time-consuming. In order to increase the accuracy of the covariance matrices and save computation time, we may use $\lim_{t\to\infty} \mathbf{P}_t^b$ for one common clipping height, $\mathbf{c}$, to use at every time step in case we can obtain the limit, instead of using $\mathbf{P}_t^b$ at each time t. If we let $\mathbf{P}_\infty$ be the unknown $n \times n$ true covariance matrix at $t = \infty$, then we have $\mathbf{P}_\infty = \lim_{M\to\infty, t\to\infty} \mathbf{P}_t^b$. When M is sufficiently large, we can assume that $\lim_{t\to\infty} \mathbf{P}_t^b \approx \mathbf{P}_\infty$. We show in the next sections that the sample covariance matrix converges to its limit in a one-dimensional linear system, and that the average of the sample covariance matrix is used as an alternative to a limit in our multidimensional nonlinear system.

2.3 One-dimensional Linear System

In this section we demonstrate our robust ensemble Kalman filter using a one-dimensional linear system.

To illustrate the effect of outliers in a one-dimensional linear system, we assume that the system equation and the observation equation are given by Eqs. (2.3) and (2.4) respectively. These simple equations have been used by Meinhold and

Singpurwalla (1983). The estimate of the classical ensemble Kalman filter (1.3) becomes

$$\bar{x}_t^a = \bar{x}_t^b + P_t^b(P_t^b + 1)^{-1}(y_t - \bar{x}_t^b),$$

given that the observation error variance is 1.

We demonstrate the performance of the robust ensemble Kalman filter to this linear system using twenty-member ensembles and a variance inflation factor of 1.1. The limit of the sample variance of the ensembles, P_t^b, of 1.63 is used to determine the clipping height, c. We use 500 replications for graphical representations with boxplots (Tukey, 1970). The efficiencies $\delta = 0.9$, 0.8 and 0.7, respectively, correspond to the clipping heights $c = 2.19$, 1.60 and 1.21 when we Huberize the observations. The same efficiencies correspond to the clipping heights $c = 4.40$, 3.71 and 3.21 when we discard the observations. The radii $r = 0.001$, 0.005 and 0.01 respectively correspond to the clipping heights $c = 4.24$, 3.48, and 3.14 when we Huberize or discard observations.

To see the impact of additive outliers, we suppose that the additive outliers with $\xi_t = 8$ are present in the data at time $t = 31$ and 32. Fig. 2.2 shows the boxplots of the bias versus efficiency for the EnKF and two REnKFs for the linear system. The efficiencies $\delta = 0.7, 0.8$, and 0.9 are used. At time $t = 31$, and 32, where the additive outliers occur, the classical EnKF has a huge bias, while the two REnKFs have smaller bias than the classical EnKF. Regarding the error variance, Huberizating the outliers is better than discarding the outliers at a fixed efficiency. Where no outliers occur at $t = 30$, the Huberization makes the error variance larger but the discarding filter makes it even larger. As the efficiency decreases, that is, the corresponding clipping value, c, decreases, the error variance increases but the bias

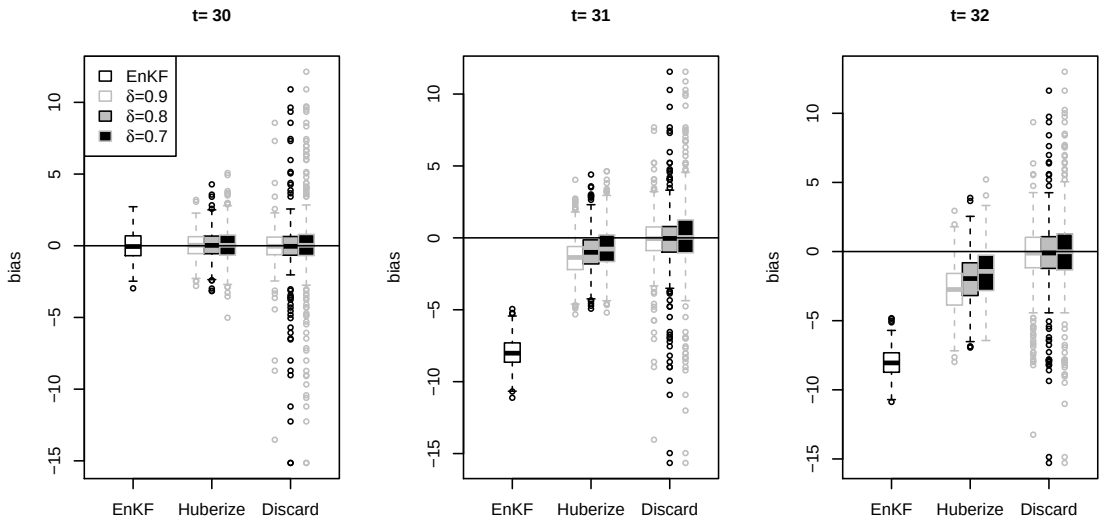

Figure 2.2: Bias versus efficiency for the EnKF and two REnKFs for a one-dimensional linear system, when the additive outliers with $\xi_t = 8$ occur only at times $t = 31$ and 32.

of the robust estimators reduces.

Fig. 2.3 shows the boxplots of the bias versus radius r in the same situation of the addtive outliers above. We use the radii of $r = 0.001, 0.005$, and 0.01. Similar to the case of the efficiency, the Huberization with radius makes the estimation bias smaller than the classical EnKF and makes the error variance smaller than the discarding. As the radius increases and so the correponding clipping value, c, decreases, the bias of the two robust estimators shrinks. The bias of the Huberization in this figure is larger than that in Fig. 2.2, since the clipping heights according to the radii we use in this figure are larger than those according to the efficiencies we use in Fig. 2.2.

The left panel in Fig. 2.4 is one of 500 sample paths in Fig. 2.2, showing the trajectory of the true state, the traditional ensemble Kalman filter, and the two robust ensemble Kalman filters with efficiency $\delta = 0.9$. The right panel in Fig.2.4 is

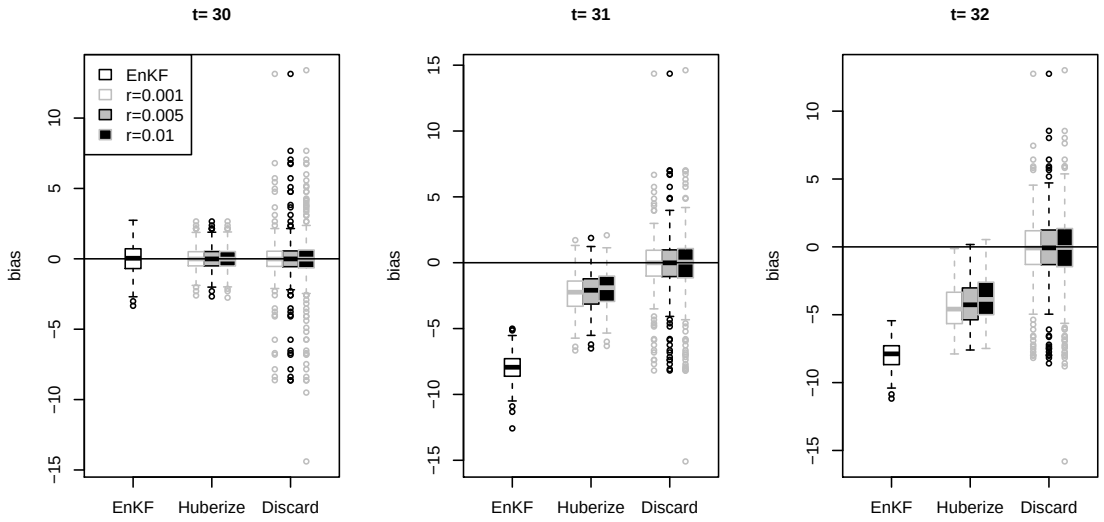

Figure 2.3: As in Fig. 2.2, but for bias versus radius.

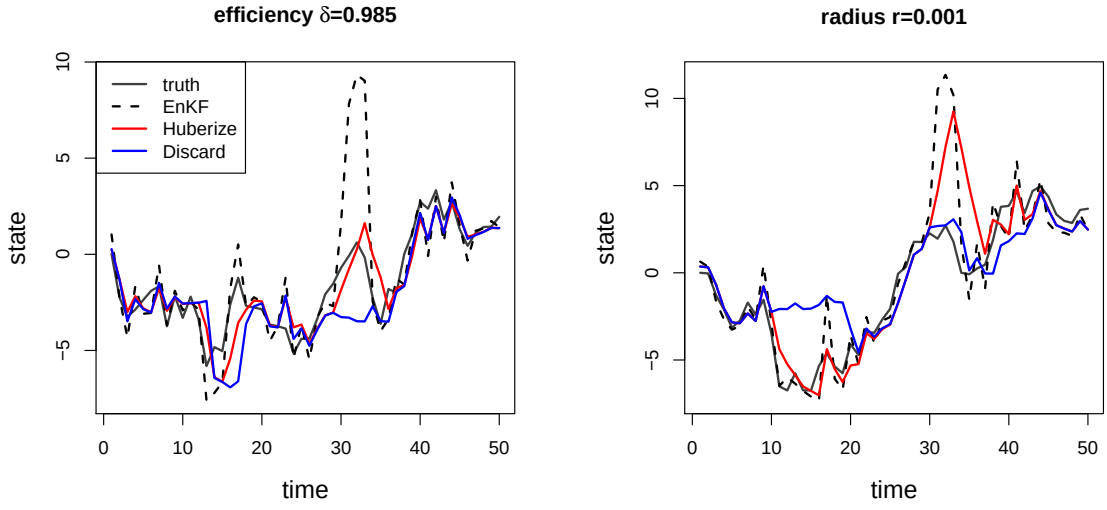

Figure 2.4: The true states, EnKF, and two REnKFs with a (left) efficiency $\delta = 0.985$ and a (right) radius $r = 0.001$, respectively, for a one-dimensional linear system. The additive outliers with $\xi_t = 8$ occur at times $t = 31$, 32 and 33.

one of 500 sample paths of Fig. 2.3, displaying the trajectories of the true state, the EnKF, and the two REnKFs with radius $r = 0.001$. The both panels exhibit that the additive outliers occurring at $t = 31, 32$ and 33 have a negative influence on the state estimation for the classical EnKF. At a fixed efficiency or at a fixed radius, the Huberization provides preciser or stabler estimation than the discarding, while both of the Huberization and the discarding have smaller jumps in the state estimation at the times of the outliers than the traditional ensemble Kalman filter has. At a efficiency $\delta = 0.9$, the discarding filter removes the jump entirely, coinciding with a bias of zero which was shown in Fig. 2.2. For a radius $r = 0.001$, while the state estimation of discarding outliers is precises than the Huberization when the outliers occur, it is impreciser than the Huberization in the absence of outliers between $t = 10$ and 20. It agrees with Fig. 2.3 illustrating that dropping outliers with the radius increases the error variance regardless of the presence or absence of outliers.

To examine the effect of innovations outliers, we suppose that the innovation outliers with $k_t = 25$ with a contamination probability of $\alpha = 0.2$ occur at times $t = 31$ and 32. Fig. 2.5 shows the boxplots of the bias versus efficiency, δ. The efficiencies we use are $\delta = 0.9$, 0.8, and 0.7. Fig. 2.6 shows the boxplots for the bias versus radius r. The used radii are $r = 0.001$, 0.005, and 0.01. Both figures illustrate that the innovation outliers occurring at times $t = 31$ and 32 force the classical EnKF to have the large error variance, while they make the bias stay at zero for both classical and robust filters, because the innovations outliers are set to have zero means. When the innovations outliers occur, Huberizing outliers is superior to dropping them and to the classical EnKF in terms of error variance, while dropping outliers makes the error variance even larger than the classical EnKF does. Regardless of the presence or absence of outliers, getting rid of outliers makes the error variance go as far as to be larger than that of the classical EnKF. The

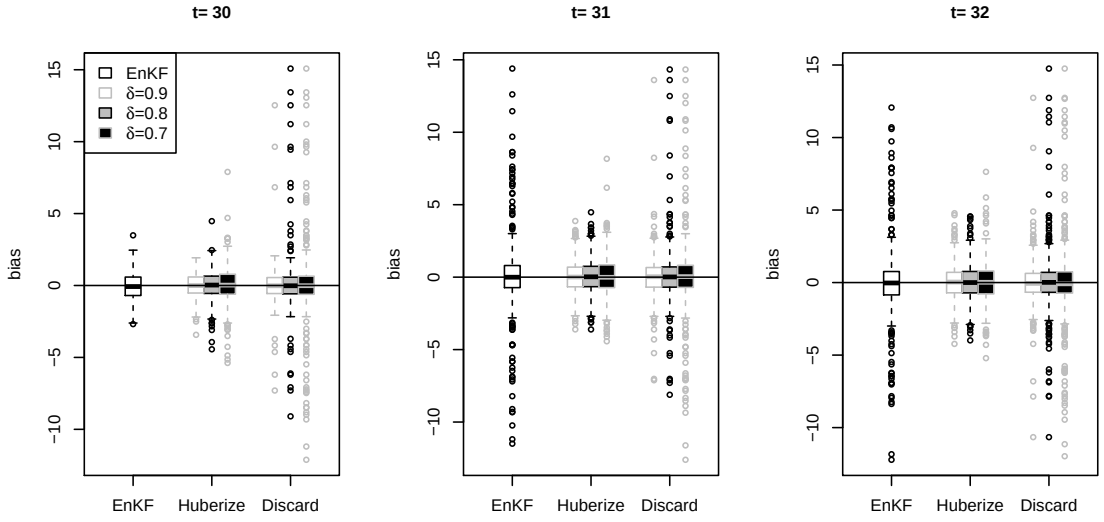

Figure 2.5: As in Fig. 2.2, but for innovations outliers with $k_t = 25$ and a probability of contamination $\alpha = 0.2$ occurring only at times $t = 31$ and 32.

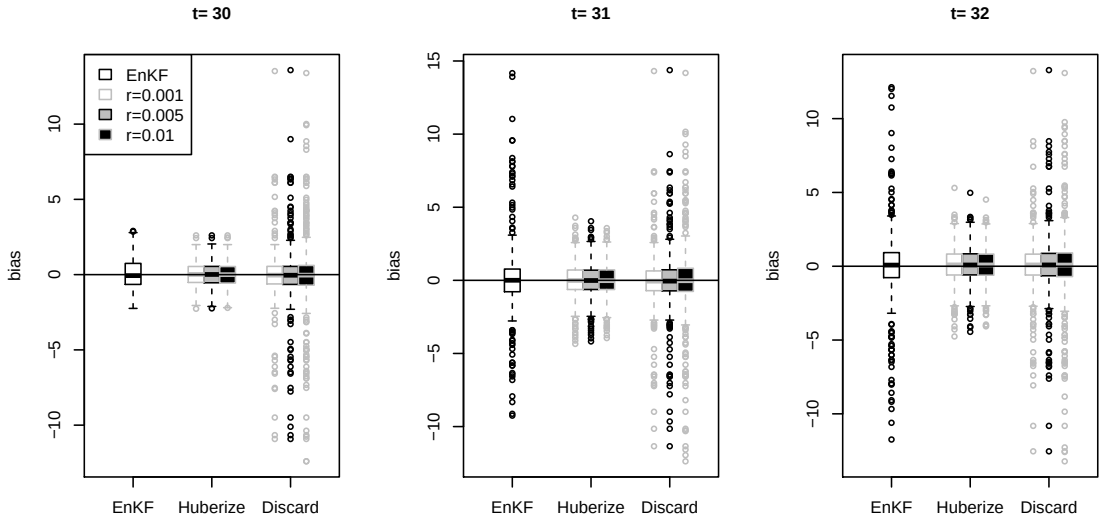

Figure 2.6: As in Fig. 2.5, but for bias vs radius.

explanation for this behavior is that a clipping function with proper clipping heights truncates observations safely but a clipping function with too small clipping heights clips observations too much: in the expression

$$\hat{\mathbf{x}}_t^a = \bar{\mathbf{x}}_t^b + \mathbf{K}_t G_{\mathbf{c}}(\mathbf{y}_t + \boldsymbol{\xi}_t - \mathbf{H}_t \bar{\mathbf{x}}_t^b),$$

the clipping function $G_{\mathbf{c}}$ cuts, in addition to $\boldsymbol{\xi}_t$, a significant portion of $\mathbf{y}_t - \mathbf{H}_t \bar{\mathbf{x}}_t^b$. Therefore, as the corresponding clipping height, c, decreases, the error variance decreases to a point but then increases again. The middle panel in Fig. 2.5 shows that decreasing efficiency, δ, that is, clipping much of outliers makes the Huberizating filter and the discarding one have larger error variance. This is because the corresponding clipping heights for both clipping functions are beyond the point, where the error variance starts to increase. On the other hand, the middle panel in Fig. 2.6 shows that increasing radius, δ, makes the error variance of the Huberization decrease but makes that of discarding increase. This implies that only for the Huber function, the corresponding clipping heights to the used radius are beyond the conversion point that begins to make the error variance larger. The efficiency, δ, gives a smaller error variance than the radius, r, does, because it yields a larger clipping value compared to the radius and as such does not clip much. When no innovations outliers occur, the two robust ensemble Kalman filters have the error variances which is equal to or larger than the traditional EnKF.

2.4 Multidimensional Nonlinear System

In this section we demonstrate our robust ensemble Kalman filter using the 40-variable Lorenz model, which is a well-known nonlinear atmospheric system.

2.4.1 The Lorenz model

We modify the 40-variable nonlinear dynamical system of Lorenz and Emanuel (1998) by adding a random model error term, dw_i. Then, the model equation is given by

$$dx_i = \{(x_{i+1} - x_{i-2})x_{i-1} - x_i + F\}dt + dw_i, \quad i = 1, \ldots, 40,$$

where dw_i is a scalar from a Gaussian distribution with a zero mean and variance of 0.05, $F = 8$, and the boundary conditions are assumed to be periodic. We use a fourth-order stochastic Runge-Kutta scheme with a time step of 0.05 nondimensional units to integrate the model. The background ensemble members are initialized from random fields and integrated for 500 steps. Each state variable is observed directly, and observations having uncorrelated errors are assimilated at every time step. The observation equation follows

$$(y_{t,1}, \ldots, y_{t,40})^T := \mathbf{y}_t = \mathbf{x}_t + \boldsymbol{\epsilon}_t,$$

where $\boldsymbol{\epsilon}_t$ is zero-mean white noise with variance $\mathbf{R} = 0.05 \cdot \mathbf{I}_{40}$, and $\mathbf{I}_{40}$ is the identity matrix of size 40. We integrated the model forward for 190 time steps and discarded a transient period which is the first 100 time steps. Twenty-member ensembles and a localization constant of 15 and ensemble inflation factor of 1.07 are used (Whitaker and Hamill 2002). Experiments were conducted using the EnKF and REnKF with perturbed observations.

2.4.2 Choice of the clipping height for the Lorenz model

We discuss how to choose the clipping height, $\mathbf{c}$, and investigate the behavior of the robust ensemble Kalman filter for the Lorenz model. We use the average of the sample background covariance matrix, $\mathbf{P}_t^b$, from $t = 101$ to 300 of $M = 10,000$ ensemble members to select a 40-dimensional clipping height vector, $\mathbf{c}$, based on a Monte Carlo integration method. Fig. 2.7 illustrates the 21-st column of the averaged sample background covariance matrix. The sample background covariance matrices

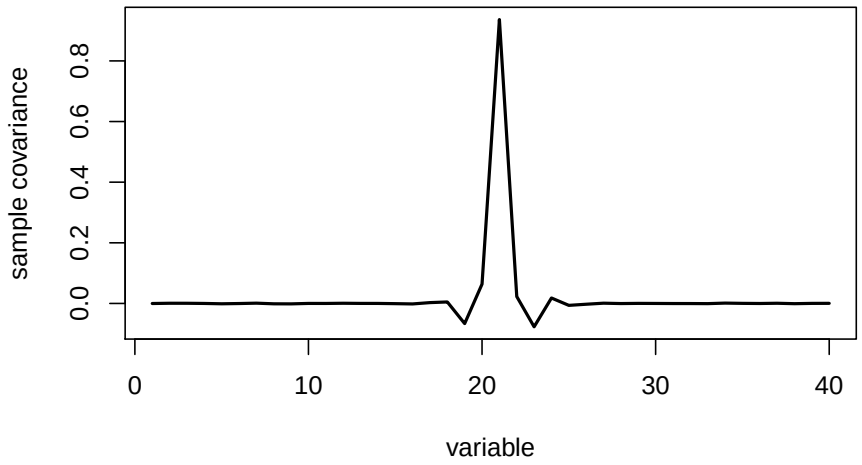

Figure 2.7: The average sample ensemble covariances between variable 21 and other variables using $10,000$ ensemble members from $t = 101$ to 300.

were computed by running the model forward and assimilating the observations.

Since the dynamics of the model, the distribution of the observations, and the observation error statistics are homogenous, all components of the clipping height vector $\mathbf{c}$ have very similar values. The radii $r = 0.001$, 0.01, and 0.05 respectively

correspond to the clipping heights 2.7, 2, and 1.44. The efficiencies $\delta = 0.99$, 0.985, and 0.98 respectively correspond to the clipping heights 0.55, 0.32, and 0.16 when we Huberize observations, and they respectively correspond to the clipping heights 1.8, 1.43, and 1.06 when we discard observations.

2.4.3 The effects of outliers

To see the effect of additive outliers in the Lorenz model, we assume that additive outliers with $\xi_t = 10$ occur for neighboring variables 11, 12 and 13, at time steps $t = 71$ and 72. Fig. 2.8 shows the boxplots of the bias versus efficiency in the presence of additive outliers for variable 11 in the Lorenz model. In this subsection, we use

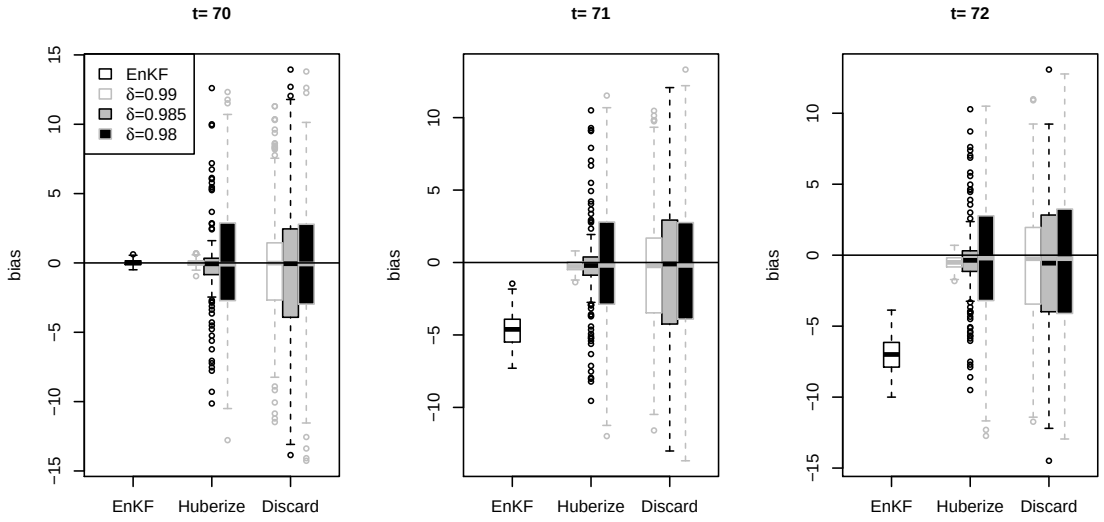

Figure 2.8: Bias versus efficiency of the EnKF and two REnKFs for variable 11 of the Lorenz model. The additive outliers $\xi_t = 10$ occur at variables 11, 12 and 13 at times $t = 71$, 72 and 73.

200 replications for graphical representations with boxplots. The Huberization and

the discarding filters greatly reduce the estimation bias at the expense of the error variance. On the other hand, the state estimation with the traditional EnKF is degraded by the additive outliers. The outliers at time $t = 71$ have a negative effect on the state estimation with the EnKF for the next time step $t = 72$. Therefore, the estimation bias at time $t = 72$ is larger than that at time $t = 71$.

Fig. 2.9 shows the boxplots of the bias versus radius in the presence of additive outliers with $\xi_t = 10$ for variable 11 in the Lorenz model. We use the radii $r = 0.001$,

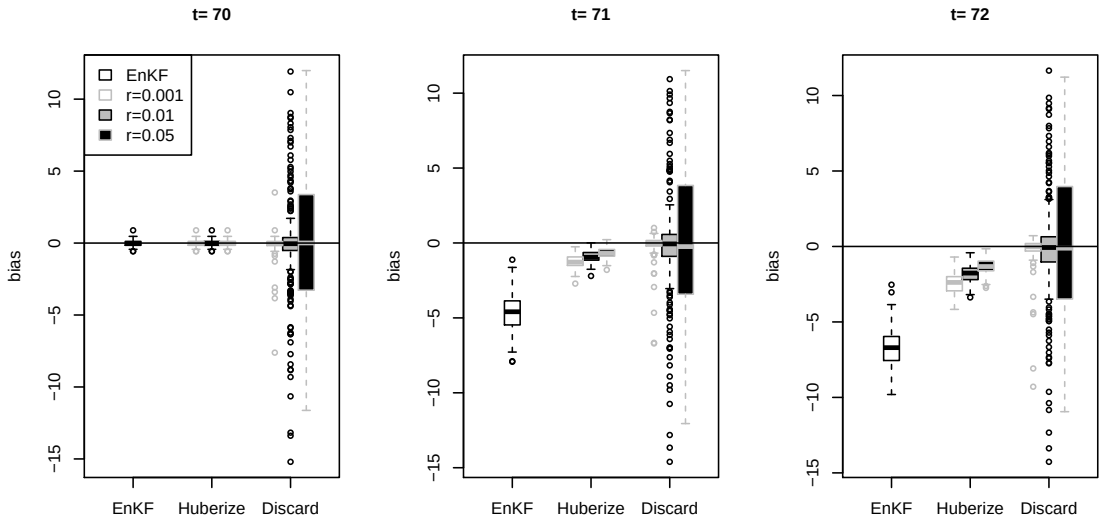

Figure 2.9: As in Fig. 2.8, but for bias versus efficiency.

0.01, and 0.05. When we discard the outliers with these radii, the error variances are still huge, but when we Huberize the outliers with the same radii, the error variances become less than those with the EnKF. As the clipping value decreases, that is, as the radius increases, the bias for the robust filters gets closer to zero. The discarding filter forces the bias to go to zero faster than does the Huberization filter. Similar

to the behavior observed in the one-dimensional linear system, the error variance decreases to a point but then it increases again as the clipping value, $\mathbf{c}$, decreases, since a proper clipping height truncates gross observations safely but a too small clipping height clips observations too much. Such aggressive clipping results in zero bias, which causes a large error variance of the state estimates. However, the rate of change of the error variance is different for the two robust ensemble Kalman filters. The discarding filter is more aggressive and its error variance therefore increases faster than does the Huberization filter. The bias for the Huberization increases from time $t = 71$ to 72 because the outliers are carried over and not perfectly removed. Once the outliers disappear, the bias then begins to recover to zero.

The left panel in Fig. 2.10 is one of 200 replications in Fig. 2.8, illustrating the time evolution of a component of the state vector for the true state, the traditional ensemble Kalman filter, and the two robust ensemble Kalman filters with a efficiency $\delta = 0.985$. Coinciding with the large error variance illustrated in Fig. 2.8, the Huberization estimates the state imprecisely, while the discarding filter estimates the state more imprecisely. The error variance is large at a quite large efficiency $\delta = 0.98$, since the maximum relative efficiency of each component of a state is 0.9747, which is obtained by completely ignoring the data. As one of 200 replications in Fig. 2.9, the right panel in Fig. 2.10 displays the time evolution of a component of the state vector for the true state, the traditional ensemble Kalman filter, and the two robust ensemble Kalman filters with a radius $r = 0.01$. From this figure, the Huberization is definitely more accurate than the discarding at the fixed radius $r = 0.01$. It does not matter weather the outliers occur or not.

To investigate the effect of innovations outliers, we assume that the observation errors come from Gaussian distribution with zero mean and extreme variance. We assume that the innovations outliers with $k_t = 100$ and a contamination probability of

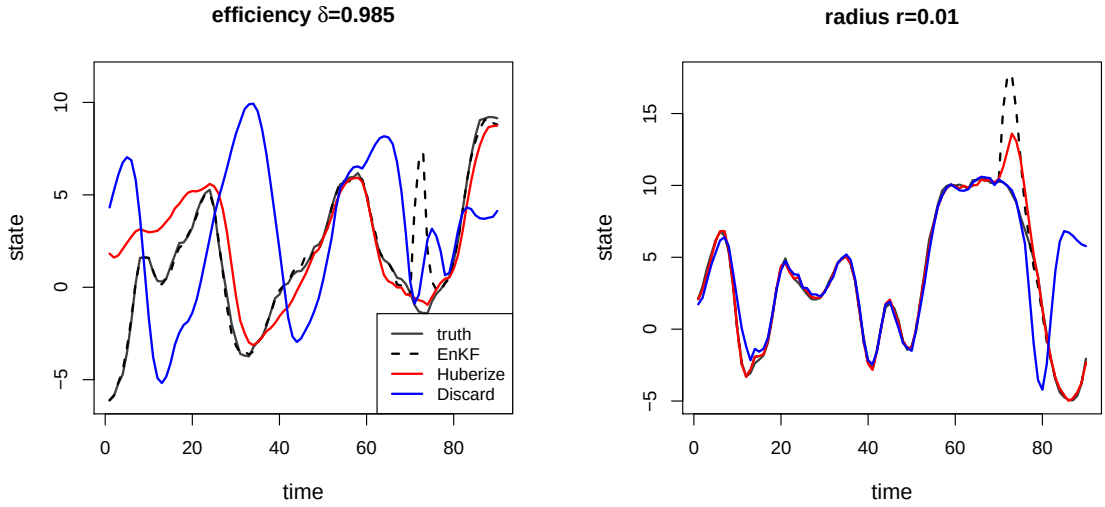

Figure 2.10: The true values, EnKF, and two REnKFs with a (left) efficiency $\delta = 0.985$ and a (right) radius $r = 0.01$, respectively, for variable 11 in the Lorenz model. The additive outliers with $\xi_t = 10$ occur at variables 11, 12 and 13 at times $t = 71$, 72 and 73.

$\alpha = 0.2$ occur at variables 11, 12 and 13 at time steps $t = 71$ and 72. Fig. 2.11 shows the boxplots of the bias versus efficiency for the EnKF and the two REnKFs in the presence of innovations outliers at variable 11 in the Lorenz model. The efficiencies $\delta = 0.99$, 0.985, and 0.98 are used. The Huberization with $\delta = 0.99$ outperforms the others, that is, it not only maintain small error variance when no outliers occur but also reduces the error variance when the outliers occur. The figure shows that the Huberization is less influenced by the efficiency, since a fixed efficiency makes the discarding have a larger error variance than the Huberization has.

Fig. 2.12 shows the boxplots of the bias versus radius in the presence of the same innovations outliers for the same variable. Such extremely large observation errors compel the traditional EnKF to make a large error variance, while the estimation bias is zero. For $r > 0$ and $\delta < 1$, the bias stays at zero but the error variance decreases

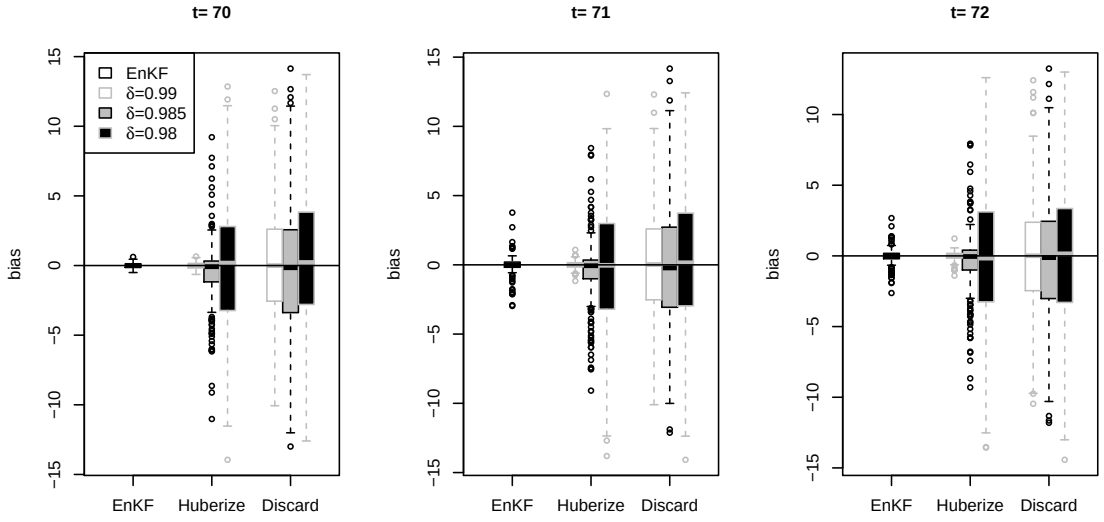

Figure 2.11: As in Fig. 2.8, but for innovations outliers with $k_t = 100$ and a contamination probability of $\alpha = 0.2$.

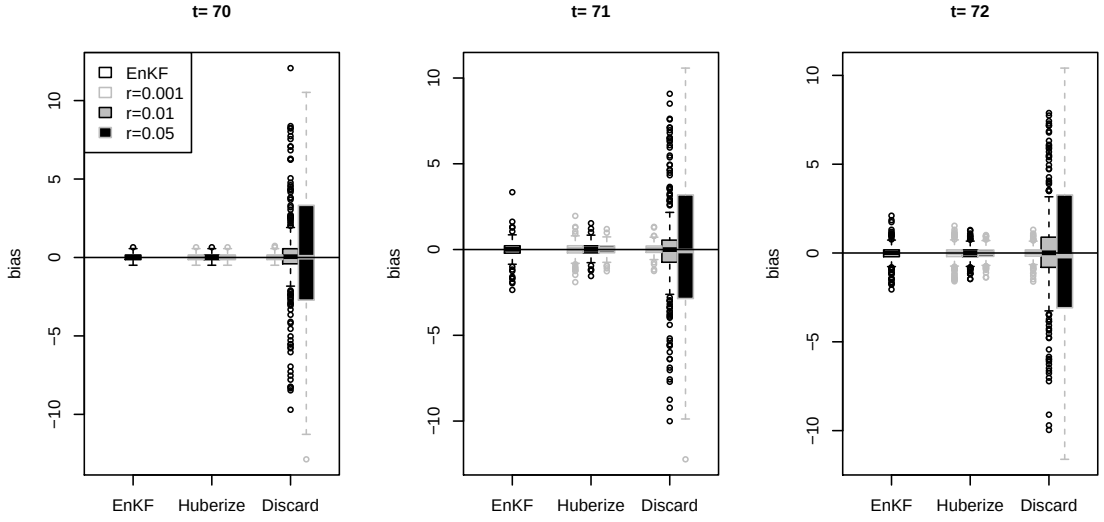

Figure 2.12: As in Fig. 2.11, but for bias versus radius.

to a certain point and then increases again as the clipping height decreases. With a fixed efficiency or a fixed radius, the Huberization experiences a large error variance slower than the discarding. At $t = 70$ when no outliers occur, both robust ensemble Kalman filters experience a loss of accuracy.

Finding the proper clipping values for a data assimilation system that assimilates many types of observations using a complex model is expected to be a labor intensive process. There is no reason to believe, however, that the process would be more challenging or would require more work than determining the parameters of the quality control procedures currently used in operational numerical weather prediction. In fact, the parameters used in the current operational systems should provide invaluable information about the gross errors in the different types of observations, which could be used as guidance for the selection of the clipping values.

3. LOCALIZATION FOR MULTIPLE STATE VARIABLES

3.1 Introduction

The components of the finite-dimensional state vector of a numerical model of the atmosphere are defined by the spatial discretization of the state variables considered in the model. An ensemble-based Kalman filter data assimilation scheme treats the finite-dimensional state vector as a multivariate random variable and estimates its probability distribution by an ensemble of samples from the distribution. To be precise, an EnKF scheme assumes that the probability distribution of the state is described by a multivariate normal distribution and it estimates the mean and the covariance matrix of that distribution by the ensemble (sample) mean and the ensemble (sample) covariance matrix. The estimate of the mean and the estimate of the covariance matrix of the analysis distribution are obtained by updating the mean and the covariance matrix of a background (prior) distribution based on the latest observations. The background distribution is represented by an ensemble of short-term forecasts from the previous analysis time. This ensemble is called the background ensemble.

Because the number of background ensemble members that is feasible to use for a realistic atmospheric model is small, the estimates of weak covariances (the entries with small absolute values in the background covariance matrix) tend to have large relative estimation errors. These large relative errors have a strong negative effect on the accuracy of an EnKF estimate of the analysis mean. The standard approach to alleviate this problem is to apply a physical-distance-dependent localization to the sample background covariances before their use in the state update step of the EnKF. In essence, localization is a method to introduce the empirical knowledge,

that the true background covariances tend to rapidly decrease with distance, into the state estimation process.

Over the years, many different localization methods have been proposed (e.g. Houtekamer and Mitchell, 1998, 2001; Hamill et al., 2001; Whitaker and Hamill, 2002; Ott et al., 2004; Hunt et al., 2007; Anderson, 2007; Buehner and Charron, 2007; Bishop and Hodyss, 2007, 2009a,b; Jun et al., 2011; Anderson and Lei, 2013; Lei and Anderson, 2014). The focus of the present paper is on the family of schemes, which localize the covariances by taking the Schur (Hadamard) product of the sample background covariance matrix and a correlation matrix of the same size, whose entries are obtained by the discretization of a distance-dependent correlation function with local (compact) support (e.g. Houtekamer and Mitchell, 2001; Hamill et al., 2001; Whitaker and Hamill, 2002). Such a correlation function is usually called a *localization* or *taper function*. Beyond a certain distance, all localization functions become zero, forcing the filtered estimates of the background covariance between state variables at locations that are far apart in space to zero. The latter property of the filtered background covariances can also be exploited to increase the computational efficiency of the EnKF schemes.

A realistic atmospheric model has multiple scalar state variables (e.g., temperature, coordinates of the wind vector, surface pressure, humidity). Thus it is important to choose the localization function such that it results in a positive-definite estimate of the covariance matrix for a spatially discretized multivariate state variable. Localization functions derived for the univariate case, such as those described by Gaspari and Cohn (1999), do not satisfy this criterion. This motivates us to seek rigorously derived multivariate localization functions for ensemble Kalman filtering.

In our search for proper multivariate localization functions, we take advantage of recent developments in the statistics literature. In particular, Zhang and Du

(2008) generalized covariance tapering methods for multiple state variables; Porcu et al. (2012) used radial basis functions to construct multivariate correlation functions with compact support; Du and Ma (2013) derived covariance matrix functions with compactly supported marginal and cross-covariances using a convolution approach and a mixture approach; while Bevilacqua et al. (2013) and Kleiber and Porcu (2013) constructed compactly supported correlation functions for multivariate random fields.

The rest of the chapter is organized as follows. Section 3.2 discusses the ensemble Kalman filtering and univariate localization, and proposes rigorous multivariate localization. Section 3.3 describes the bivariate Lorenz-95 model we use to test our ideas and results of our numerical experiments with that model, and compares a variety of multivariate localization schemes.

3.2 Multivariate Localization

In this section we review the formulations of the EnKF, and examine the univariate localization and related issues occurring during simultaneous estimation of several state variables. Finally, we propose rigorous multivariate localization functions.

3.2.1 The EnKF update equation

Data assimilation schemes treat the spatially discretized state vector $\mathbf{x}$ as a multivariate random variable. We use the conventional notations $\mathbf{x}^b$ and $\mathbf{x}^a$ for the background and the analysis state vectors, respectively. In an EnKF scheme, the analysis mean $\bar{\mathbf{x}}^a$ is computed from the background mean $\bar{\mathbf{x}}^b$ by the update equation

$$\bar{\mathbf{x}}^a = \bar{\mathbf{x}}^b + \mathbf{K}\left(\mathbf{y}^o - \overline{\mathbf{h}\left(\mathbf{x}^b\right)}\right). \tag{3.1}$$

The function $\mathbf{h}(\cdot)$ is the observation function, which maps the finite-dimensional state vector into observables. Thus $\overline{\mathbf{h}\left(\mathbf{x}^b\right)}$ is the ensemble mean of the prediction of the observations by the background. The matrix

$$\mathbf{K} = \mathbf{P}^b\mathbf{H}^T\left(\mathbf{H}\mathbf{P}^b\mathbf{H}^T + \mathbf{R}\right)^{-1} \tag{3.2}$$

is the Kalman gain matrix, where $\mathbf{P}^b$ is the background covariance matrix, $\mathbf{H}$ is the linearization of $\mathbf{h}$ above $\bar{\mathbf{x}}^b$, and $\mathbf{R}$ is the observation error covariance matrix. The entry K_{ij} of $\mathbf{K}$ determines the effect of the j-th observation on the i-th component of the analysis mean $\bar{\mathbf{x}}^a$. Under the standard assumption that the observation errors are uncorrelated, the matrix $\mathbf{R}$ is diagonal. Hence, the way the effect of the observations is spread from the observations to the different locations and state variables is determined by $\mathbf{P}^b$ and $\mathbf{H}$. Sampling variability affects the accuracy of the information propagated in space and between the different state variables through the matrix products $\mathbf{P}^b\mathbf{H}^T$ and $\mathbf{H}\mathbf{P}^b\mathbf{H}^T$. The goal of localization is to reduce the related effects of sampling variability on the estimates of $\mathbf{K}$.

In principle, localization can be implemented by using filtered estimate of the background covariances rather than the raw sample covariances to define the matrix $\mathbf{P}^b$ used in the computation of $\mathbf{K}$ by Eq. (3.2). In practice, however, the localization is often done by taking advantage of the fact that localization affects the analysis through $\mathbf{P}^b\mathbf{H}^T$ and $\mathbf{H}\mathbf{P}^b\mathbf{H}^T$, or ultimately, through $\mathbf{K}$. In particular, because a distance d can be defined for each entry K_{ij} of $\mathbf{K}$ by the distance between the i-th analyzed variable and the j-th observation, the simplest localization strategy is to set all entries K_{ij} that are associated with a distance larger than a prescribed localization radius R ($d > R$) to zero, while leaving the remaining entries unchanged (e.g. Houtekamer and Mitchell, 1998; Ott et al., 2004; Hunt et al., 2007). Alterna-

tively, the entries K_{ij} within the localization distance ($d \leq R$) can be multiplied by a properly computed distance dependent scalar tapering factor (e.g. Anderson and Lei, 2013; Lei and Anderson, 2014).

Another approach is to localize $\mathbf{P}^b\mathbf{H}^T$ and $\mathbf{H}\mathbf{P}^b\mathbf{H}^T$ by a tapering function(e.g. Houtekamer and Mitchell, 2001; Hamill et al., 2001). The usual justification for this approach is that $\mathbf{H}$ is typically the linearization of a local interpolation function $h(\cdot)$, for which the localized matrix products provide good approximations to the products computed by using localized estimates of $\mathbf{P}^b$. Note that $\mathbf{P}^b\mathbf{H}^T$ is the matrix of background covariances between the state variables at the model grid points and at the observation locations, while $\mathbf{H}\mathbf{P}^b\mathbf{H}^T$ the matrix of background covariances between the state variables at the observation locations. Thus a distance can be associated with each entry of the two matrix products, which makes the distance dependent localization of the two products possible. The approach becomes problematic, however, when $h(\cdot)$ is not a local function, which is the typical case for remotely sensed observations (Campbell et al., 2010).

We consider the situation where localization is applied directly to the background error covariance matrix.

3.2.2 Univariate localization

The filtered covariance matrix $\mathbf{P}^b$ is obtained by computing the Schur (entry-wise) product

$$\mathbf{P}^b = \hat{\mathbf{P}}^b \circ \mathbf{C}, \tag{3.3}$$

where $\mathbf{C}$ is a correlation matrix, which has the same dimensions as the sample covariance matrix, $\hat{\mathbf{P}}^b$. A covariance matrix must be positive-definite. The filtered matrix $\mathbf{P}^b$ obtained by Eq. (3.3) satisfies this condition, because both $\hat{\mathbf{P}}^b$ and $\mathbf{C}$ are positive-definite and the Schur theorem (e.g., Bhatia, 1997) states that the Schur

product of two positive-definite matrices is also a positive-definite matrix.

The proper definition of the localization function, which ensures that $\mathbf{C}$ is positive-definite, has been thoroughly investigated for the univariate case ($N = 1$) by Gaspari and Cohn (1999). A seemingly obvious approach to extend the results of Gaspari and Cohn (1999) to the multivariate case would be to compute the entires of $\mathbf{C}$ based on a univariate correlation function, even if $\hat{\mathbf{P}}^b$ was obtained for a multivariate variable. Formally, this would be possible, because a distance d is uniquely defined for each entries of $\hat{\mathbf{P}}^b$ the same way in the multivariate case as in the univariate case. This approach, however, does not work, as it cannot guarantee the positive-definitiveness of the resulting matrix $\mathbf{C}$. As a simple example, consider the situation where the discretized state vector has only two components that are defined by two different scalar state variables at the same location (e.g., the temperature and the pressure). In this case,

$$\mathbf{C} = \begin{pmatrix} 1 & 1 \\ 1 & 1 \end{pmatrix}, \tag{3.4}$$

independently of the particular choice of the localization function. This $\mathbf{C}$ is not a proper correlation matrix: one of its two eigenvalues is zero, which implies that the matrix is not positive-definite.

3.2.3 Multivariate localization

We consider a model with N state variables. For instance, for a simple model based on the hydrostatic primitive equations, which solves the equations for the two horizontal component of the wind, the surface pressure, the virtual temperature and for a couple of atmospheric constituents. The state of the model is represented by the state vector $\mathbf{x} = (\mathbf{x}_1, \mathbf{x}_2, \ldots, \mathbf{x}_N)$, where $\mathbf{x}_i$, $i = 1, 2, \ldots, N$, represents the spatially discretized state of the i-th state variable in the model.

The sample background covariance matrix $\hat{\mathbf{P}}^b$ can be partitioned as

$$\hat{\mathbf{P}}^b = \begin{pmatrix} \hat{\mathbf{P}}^b_{11} & \hat{\mathbf{P}}^b_{12} & \cdots & \hat{\mathbf{P}}^b_{1N} \\ \hat{\mathbf{P}}^b_{21} & \hat{\mathbf{P}}^b_{22} & \cdots & \hat{\mathbf{P}}^b_{2N} \\ \cdots & \cdots & \cdots & \cdots \\ \hat{\mathbf{P}}^b_{N1} & \hat{\mathbf{P}}^b_{N2} & \cdots & \hat{\mathbf{P}}^b_{NN}, \end{pmatrix}. \tag{3.5}$$

The entries of the submatrices $\hat{\mathbf{P}}^b_{ii}$, $i = 1, \ldots, N$, are the marginal-covariances for the i-th state variable. In practical terms, if the i-th state variable is the virtual temperature, for instance, each diagonal entry of $\hat{\mathbf{P}}^b_{ii}$ represents the sample variance for the virtual temperature at a given model grid point, while each off-diagonal entry of $\hat{\mathbf{P}}^b_{ii}$ represents the sample covariance between the virtual temperatures at a pair of grid points. Likewise, the entries of $\hat{\mathbf{P}}^b_{ij}$, $i \neq j$, are the sample cross-covariance between the grid point values of the i-th and the j-th state variables at pairs of locations, where the two locations for an entry can be the same grid point.

We consider matrix-valued localization functions, $\boldsymbol{\rho}(d) = \{\rho_{ij}(d)\}_{i,j=1,\ldots,N}$, which are continuous functions of d. The component $\rho_{ij}(d)$ of $\boldsymbol{\rho}(d)$ is the localization function used for the calculation of the covariances included in the sub-matrix $\mathbf{P}^b_{ij}$ of $\mathbf{P}^b$. Each entry of $\mathbf{C}$ is computed by considering the value of the appropriate component of $\boldsymbol{\rho}(d)$ for the two state variables and the distance d associated with the related entry of $\hat{\mathbf{P}}^b$. If the matrix $\boldsymbol{\rho}(d)$ is positive-definite and its components are proper correlation functions, the resulting matrix $\mathbf{C}$ is a proper correlation matrix.

We consider two approaches to construct positive-definite (full rank) matrix-valued localization functions $\boldsymbol{\rho}(d)$. The first proposed method takes advantage of the knowledge of a proper univariate localization function, $\tilde{\rho}$. As shown before, using the same localization function for each $\mathbf{P}^b_{ij}$ may result in rank deficiency. This

motivates the choice $\boldsymbol{\rho} = \tilde{\rho}\ \mathbf{B}$, where $\mathbf{B}$ is an $N \times N$ symmetric, positive-definite matrix whose diagonal entries are one. It can be easily verified that $\boldsymbol{\rho}$ is a matrix-valued positive-definite function, which makes it a valid multivariate localization function. For instance, in the hypothetical case where the two components of the state vector are two different state variables at the same location, making the choice

$$\mathbf{B} = \begin{pmatrix} 1 & \beta \\ \beta & 1 \end{pmatrix}, \tag{3.6}$$

with $|\beta| < 1$ leads to

$$\mathbf{C} = \begin{pmatrix} 1 & \beta \\ \beta & 1 \end{pmatrix} \tag{3.7}$$

rather than Eq. (3.4) in the hypothetical case where the two components of the state vector are two different state variables at the same location. Since the eigenvalues of the matrix $\mathbf{C}$ in Eq. (3.7) are $1 \pm \beta > 0$, the matrix is positive-definite.

An attractive feature of this approach is that we can take advantage of any known univariate localization function to produce a multivariate localization function. However, the multivariate localization function from this approach is *separable* in the sense that the multivariate component (i.e. $\mathbf{B}$) and localization function (i.e. $\tilde{\rho}$) are factored. Another limitation of the approach is that the localization radius is the same for each pair of the state variables, leaving no flexibility to account for the potential differences in the correlation length for the different state vector components.

The second proposed method takes advantage of the availability of multivariate compactly supported functions from the spatial statistics literature. To the best of our knowledge, only a few papers have been published on the subject and one of

them is Porcu et al. (2012). The function class they considered was essentially a multivariate extension of the *Askey* function (Askey, 1973), $f(d;\nu,c) = \left(1-\frac{d}{c}\right)_+^{\nu}$, with $c,\nu > 0$. Here, $x_+ = \max(x,0)$ for $x \in \mathbb{R}$. For instance, a bivariate Askey function, which is a special case of the results of Porcu et al. (2012), is given by $(i,j=1,2)$

$$\rho_{ij}(d;\nu,c) = \beta_{ij}\left(1-\frac{d}{c}\right)_+^{\nu+\mu_{ij}}, \tag{3.8}$$

where $c>0$, $\mu_{12}=\mu_{21} \le \frac{1}{2}(\mu_{11}+\mu_{22})$, $\nu \ge [\frac{1}{2}s]+2$, $\beta_{ii}=1$ $(i=1,2)$, $\beta_{12}=\beta_{21}$, and

$$|\beta_{12}| \le \frac{\Gamma(1+\mu_{12})}{\Gamma(1+\nu+\mu_{12})}\sqrt{\frac{\Gamma(1+\nu+\mu_{11})\Gamma(1+\nu+\mu_{22})}{\Gamma(1+\mu_{11})\Gamma(1+\mu_{22})}}. \tag{3.9}$$

Here, s is the dimension of the Euclidean space where the state variable is defined, and $[x]$ is the largest integer that is equal to or smaller than x. It can be seen from (3.9) that, if the scalars μ_{ij} are chosen to be the same for all values of i and j, the condition on β_{12} for $\boldsymbol{\rho}$ to be valid is $|\beta_{12}| \le 1$. Note that for this choice the second method is essentially the same as the first method with the Askey function as $\tilde{\rho}$. The localization function given by (3.8) is more flexible than the functions of the first method with the Askey function as $\tilde{\rho}$ because μ_{ij} can be chosen to be different for each pair of the indexes i and j. The localization length, however, is still the same for the different pairs of the state variables.

3.3 Experiments

The goal of our numerical experiments is to test the performance of the proposed multivariate localization methods by carrying out ensemble Kalman filter on the bivariate Lorenz-95 model (Lorenz, 1995).

3.3.1 EnKF Scheme

There are many different formulations of the EnKF update equations, which have to produce not only an update of the mean, but also the ensemble of analysis perturbations that can be added to the mean to obtain an ensemble of analyses. This ensemble of analyses serves as the ensemble of initial conditions for the model integration that produce the background ensemble. In our experiments, we use the method of perturbed observations, which obtains the analysis mean and the ensemble of analysis perturbations by the equations

$$\bar{\mathbf{x}}^a = \bar{\mathbf{x}}^b + \mathbf{K}(\mathbf{y} - \mathbf{H}\bar{\mathbf{x}}^b), \tag{3.10}$$

$$\mathbf{x}_k^{a'} = \mathbf{x}_k^{b'} + \mathbf{K}(\mathbf{y}_k^{o'} - \mathbf{H}\mathbf{x}_k^{b'}),, \tag{3.11}$$

where $\mathbf{x}_k^{'}$, $k = 1, 2, \ldots, M$ are the ensemble perturbation and $\mathbf{y}_k^{o'}$, $k = 1, 2, \ldots, M$, are random draws from the probability distribution of observation errors. As the notation suggests, we consider a linear observation function in our experiments. This choice is made for the sake of simplicity and limits the generality of our findings much less than the use of an idealized model of the atmospheric dynamics.

3.3.2 Bivariate Lorenz model

The idealized model we use is the bivariate Lorenz-95 model. The model mimics the nonlinear dynamics of two linearly coupled atmospheric state variables, X and Y, on a latitude circle. The variable, X, is a "slow" variable represented by K discrete values, X_k, and Y is a "fast" variable represented by $J \times K$ discrete values. The

governing equations are

$$\frac{dX_k}{dt} = -X_{k-1}(X_{k-2} - X_{k+1}) - X_k - (ha/b)\sum_{j=1}^{J} Y_{j,k} + F, \tag{3.12}$$

$$\frac{dY_{j,k}}{dt} = -abY_{j+1,k}(Y_{j+2,k} - Y_{j-1,k}) - aY_{j,k} + (ha/b)X_k, \tag{3.13}$$

where $Y_{j-J,k} = Y_{j,k-1}$ and $Y_{j+J,k} = Y_{j,k+1}$ for $k = 1, \ldots, K$ and $j = 1, \ldots, J$. The "boundary condition" is periodic, that is, $X_{k-K} = X_{k+K} = X_K$, and $Y_{j,k-K} = Y_{j,k+K} = Y_{j,k}$. In our experiments, $K = 36$ and $J = 10$. The parameter h controls the strength of the coupling between X and Y, a is the ratio of the characteristic time scale of the slow motion of X and the fast motion of Y, b is the ratio of the characteristic amplitude of X and Y, and F is a forcing term. Following Lorenz (1995), we choose the parameters to be $a = 10$, $b = 10$, $h = 2$, and $F = 10$. We use a fourth-order Runge-Kutta time integration scheme with a time step of 0.005 non-dimensional units. Fig. 3.1 shows a typical state of the model for the selected parameters. The figure shows that the slow variable tends to drive the evolution of the fast variable: the hypothetical process represented by Y is more active (its variability is higher) for the higher values of X.

3.3.3 Experiment design

Since the estimates of the cross-covariances play a particularly important role at locations where one of the variables is unobserved, we expect the better treatment of the cross-covariances to lead to analysis improvements at locations where only X or Y is observed. This motivates us to consider an observation scenario, in which X is observed at 20% of all locations and Y is observed at 90% of those locations where X is not observed. The results from this experiment are compared to those from a control experiment, in which both X and Y are fully observed.

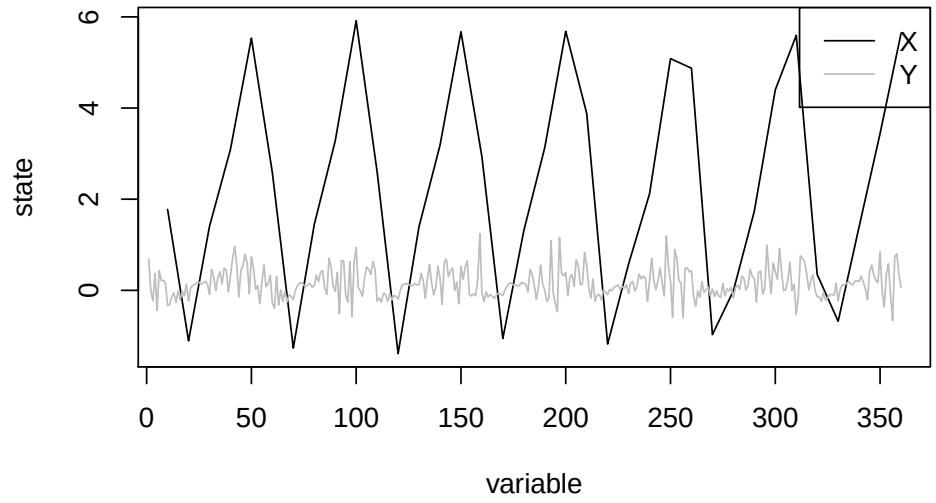

Figure 3.1: Plot of the states of the bivariate Lorenz-95 model in Eqs. (3.12) and (3.13) with $a = 10$, $b = 10$, $h = 2$, and $F = 10$ as a function of variable.

We first generate a time series of "true" model states by a 2,000 time steps long integration of the model, and then generate simulated observations by adding random observation noise of mean zero and variance of 0.005 to the the appropriate components of the "true" state at each time step. Observations are assimilated at every time steps with the help of a 20-member ensemble. The error in the analysis at a given verification time is measured by the root-mean-square distance between the analysis mean and the true state. We refer to the resulting measure as the root-mean-square error (RMSE). The probability distribution of the RMSE for the last 1,000 time steps of 100 different realization of each experiment is shown by a boxplot.

In the boxplot figures described in the next section, we compare the RMSE for four different type localization schemes. We use the following notations to distinguish

between them in the figures:

1. S1–the bivariate sample background covariance is used without localization;

2. S2–same as S1 except that the cross covariance terms are replaced by zeros;

3. S3–a univariate localization function is used to filter the marginal-covariances, while the cross-covariance terms are replaced by zeros;

4. S4–one of the bivariate localization methods described in Section 3.2.3 is used to filter both the marginal- and the cross-covariances.

In the experiments identified by S4, we consider two different bivariate localization functions: The first one is $\boldsymbol{\rho}^{(1)}(\cdot) = \{\beta_{ij}\rho^{(1)}(\cdot)\}_{i,j=1,2}$ with $\beta_{ii} = 1$ $(i = 1, 2)$, $\beta_{ij} = \beta$ $(i \neq j)$, and $|\beta| < 1$. We use the fifth-order piecewise-rational function of Gaspari and Cohn (1999) to define the univariate correlation function $\rho^{(1)}$ in the following form,

$$\rho^{(1)}(d;c) = \begin{cases} -\frac{1}{4}(|d|/c)^5 + \frac{1}{2}(d/c)^4 + \frac{5}{8}(|d|/c)^3 - \frac{5}{3}(d/c)^2 + 1, & 0 \leq |d| \leq c; \\ \gamma(d;c), & c \leq |d| \leq 2c; \\ 0, & 2c \leq |d|, \end{cases} \tag{3.14}$$

where $\gamma(d;c) = \frac{1}{12}(|d|/c)^5 - \frac{1}{2}(d/c)^4 + \frac{5}{8}(|d|/c)^3 + \frac{5}{3}(d/c)^2 - 5(|d|/c) + 4 - \frac{2}{3}c/|d|$. This correlation function attenuates the covariances with increasing distance, setting all the covariances to zero beyond distance $2c$. If $|\beta| < 1$ and c is the same for both the marginal- and the cross-covariances, the matrix-valued function $\boldsymbol{\rho}^{(1)}$ is positive-definite and of full rank. We try various c and β values.

The second multivariate correlation function we consider, $\boldsymbol{\rho}^{(2)}$, is the bivariate Askey function described in Eq. (3.8). In particular, we use $\mu_{11} = 0$, $\mu_{22} = 2$,

$\mu_{12} = 1$, and $\nu = 3$. Due to (3.9), for $\boldsymbol{\rho}^{(2)}$, we need $|\beta_{12}| < 0.79$. Fig. 3.2 displays two univariate tapering functions: the Gaspari-Cohn function $\rho^{(1)}$ (with $c = 25$) and the Askey function $\rho_{11}^{(2)}$ (with $c = 50$, $\nu = 1, 2, 3$, and $\mu_{11} = 0$). The figure shows

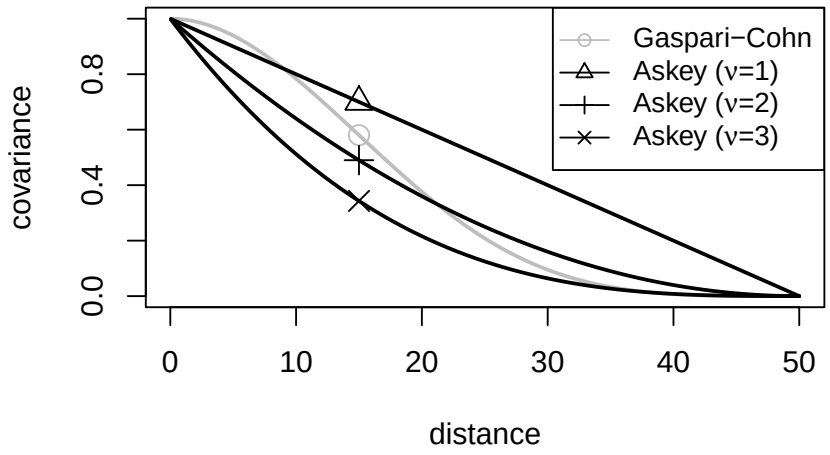

Figure 3.2: Plot of the Gaspari-Cohn function with a support of 50 ($c = 25$)and the Askey function with the same support and various shape parameters $\nu = 1, 2, 3$.

that the Gaspari-Cohn function is smoother at the origin than the Askey function with any shape parameter.

3.3.4 Result

In this subsection, we display four figures of RMSE in order to compare the four different localization schemes described in subsection 3.3.3. In each figure, we compare the Gaspari-Cohn function with the Askey function by using various supports: $50, 70, 100$, and 160.

Fig. 3.3 shows RMSEs for a variable X in scenario 1. The localization scheme S4 with $\beta = 0.005$ works better than the other schemes, since 20% of X are not enough to represent the entire of X and treatment of Y is helpful to estimate X by compensating for it. S3 with small support has large errors, since it replaces cross-covariance terms by zero and loses information in marginal-covariance terms. When support increases, the error of S3 then becomes closer to that of S2, since S2 is identical to S3 with infinitely large support. For the localization scheme S3 which ignores the cross-covariance, a smaller support produces a larger RMSE, while for the localization scheme S4 which treats the cross-covariance, a smaller support makes a smaller RMSE.

Fig. 3.4 shows RMSEs for a variable Y in scenario 1. The figure shows that when supports are 50 and 70, the localization S3 performs the best in terms of the error. It is opposite to the case of the state variable X, which is dominant over Y. Given the used set of model parameters, one variable of X is closely associated with 10 variables of Y in the way that a value of X has an influence on the fluctuation of the associated variables of Y. From 10 variables of Y which fluctuate much, the associated variable X can be expected to have a larger value. On the other hand, if 10 variables of Y fluctuates less, the associated variable of X can be expected to have a small value. Therefore, in scenario 1 where we observe a small portion of the dominant variable X, maintaining information in the cross-covariance terms between X and Y improves the accuracy of the estimation of X. A value of X, however, does not give the actual value of Y, while giving us information of how much the associated variables of Y fluctuate. Thus the localization method S4, which pays attention to the cross-covariance, does not improve the precision of estimation. The Askey function produces smaller errors than the Gaspari-Cohn function does due its flexibility depending on shape parameters.

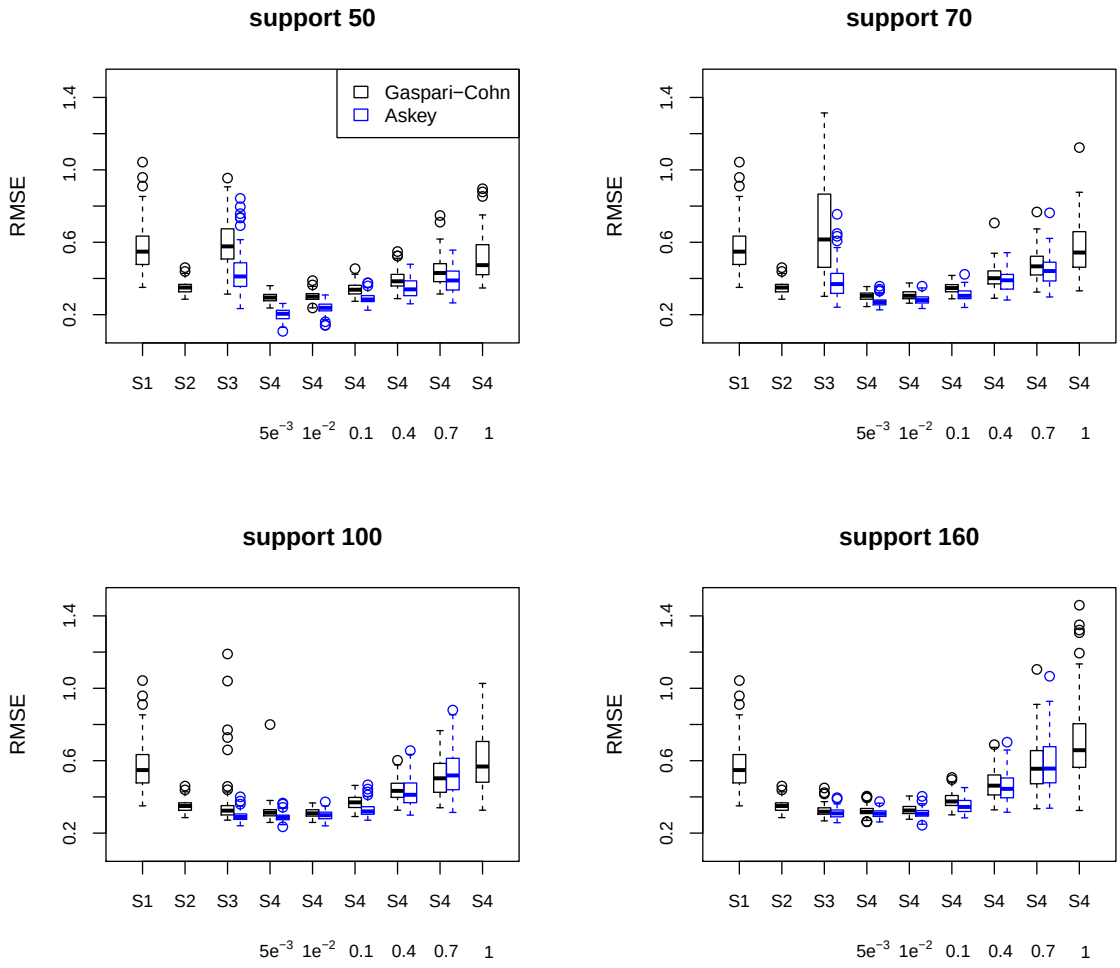

Figure 3.3: Boxplot of RMSEs for a variable $\mathbf{X}$ in scenario 1 using (black) the Gaspari-Cohn function and (blue) Askey function with various supports. Boxplots left to right in each panel are for localization schemes S1, S2, S3 and for S4 with various β. The values of β are below S4.

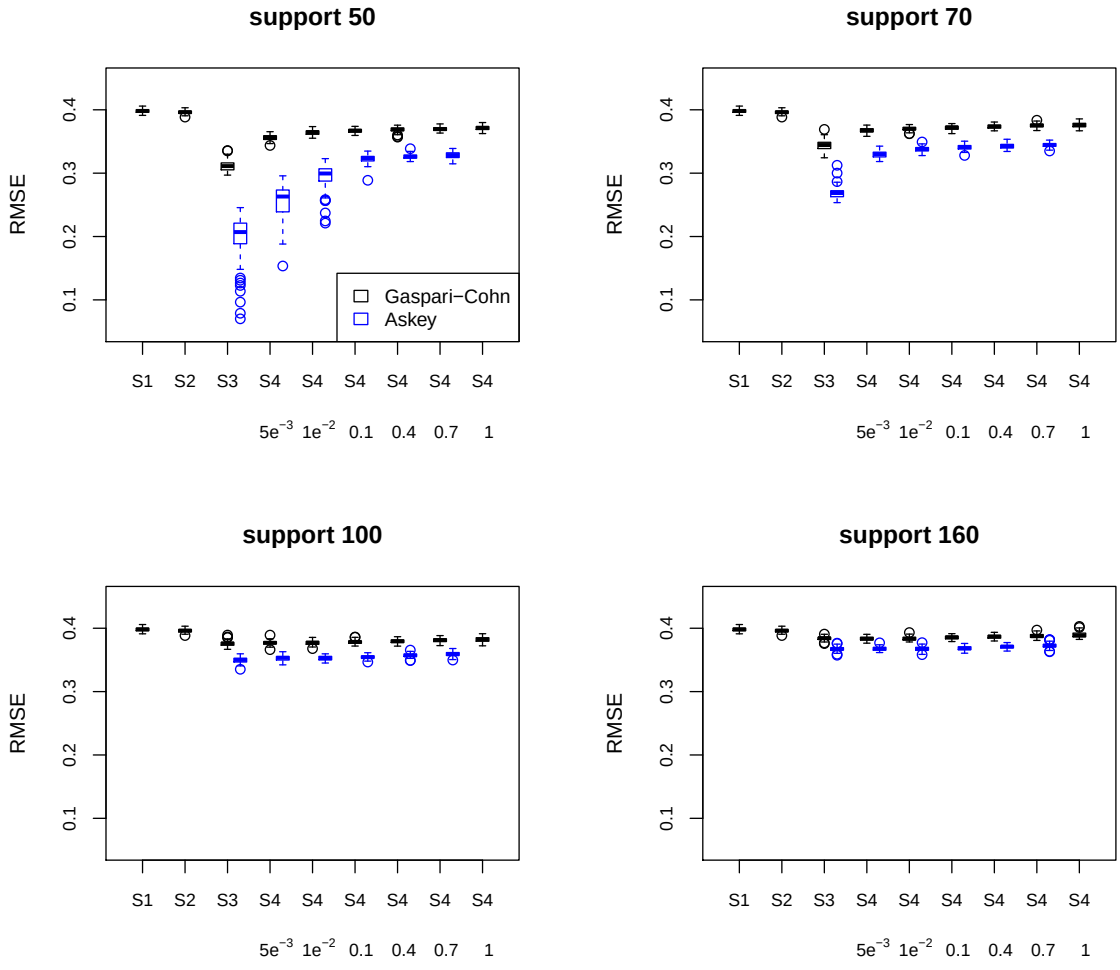

Figure 3.4: As in Fig. 3.3, but for a variable Y.

Fig. 3.5 shows RMSEs for a variable X in scenario 2 where we have full observations of both X and Y. S4 with smaller β produces the smallest RMSE. Different

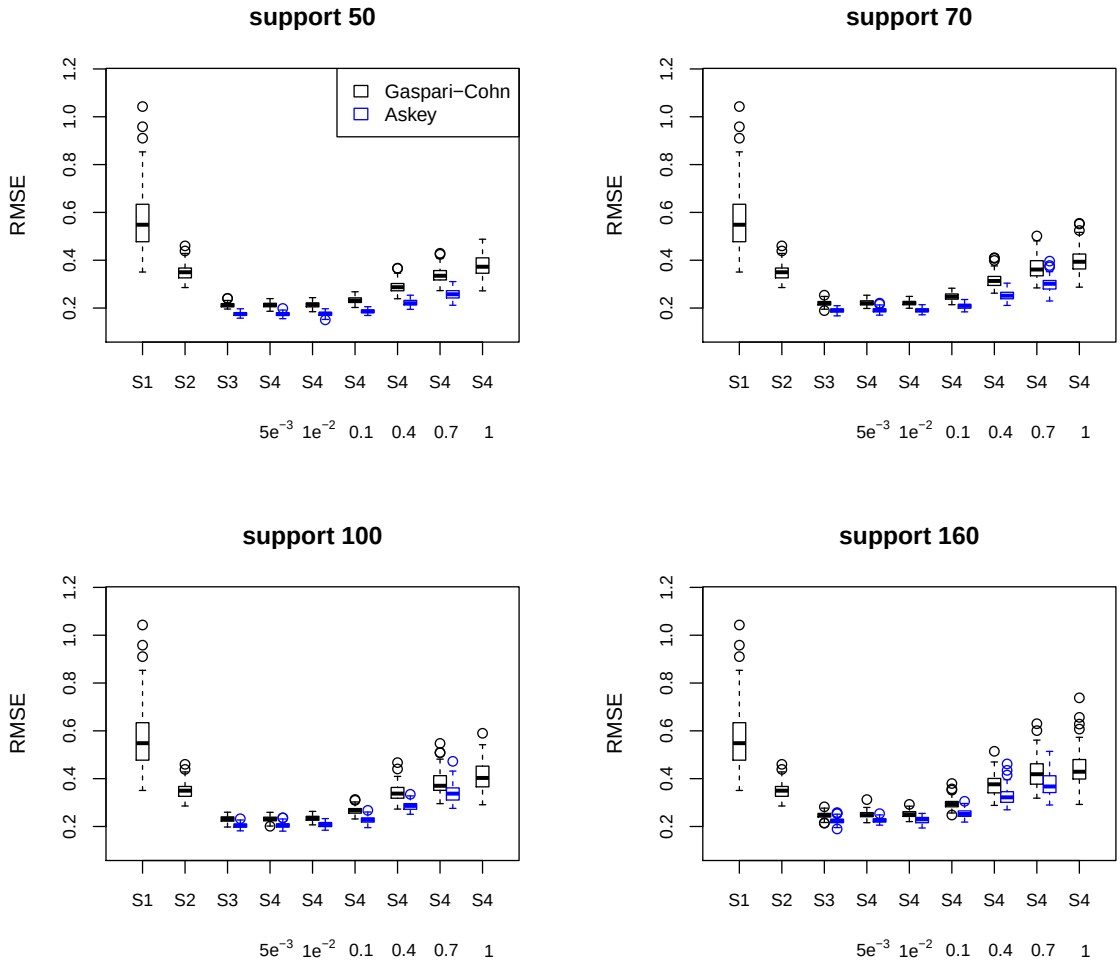

Figure 3.5: As in Fig. 3.3, but for scenario 2.

from scenario 1, S3 has smaller RMSE than S2 for all the supports. S3 causes a loss of information since it substitutes the cross-covariance terms for zero, but it uses full knowledge of the two state variables.

Fig. 3.6 shows RMSEs for a variable Y in scenario 2. The localization schemes

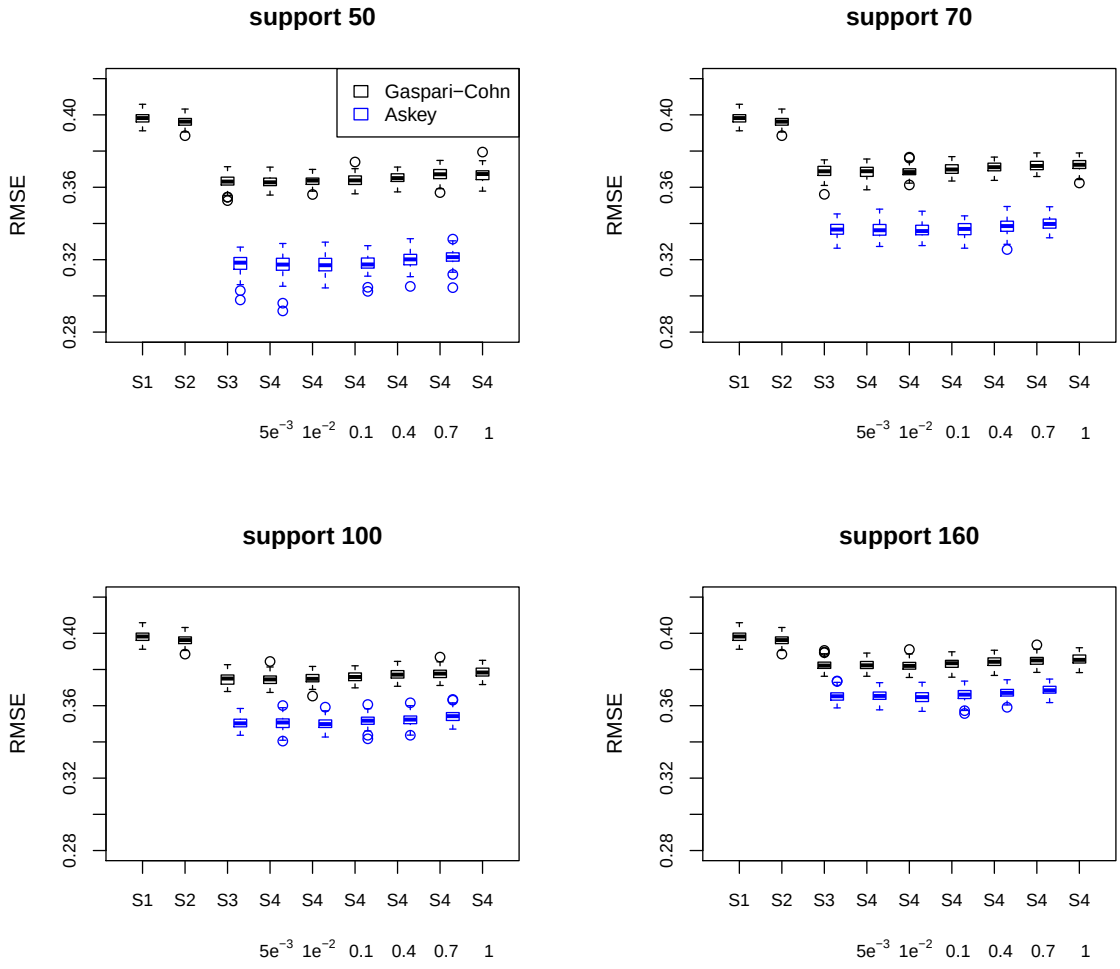

Figure 3.6: As in Fig. 3.5, but for a variable Y.

S3 and S4 with any β have similar RMSE. The bivariate Askey correlation function gives smaller errors than the Gaspari-Cohn correlation function, since the Askey correlation function is adaptable depending on shape parameter as well as support parameter, while the Gaspari-Cohn function depends only on localization parameter.

4. MULTIVARIATE ROBUST ENSEMBLE KALMAN FILTER

4.1 Introduction

Ruckdeschel (2010) introduced a method to make the Kalman filter (KF) robust to gross observation errors in a linear system. The most important feature of the robust Kalman filtering (RKF) scheme is that it clips the magnitude of an innovation (observation prediction error which is a discrepancy between an observation and its predicted value) at an upper bound when the magnitude of the innovation is found to be larger than the upper bound. The drawback is that in case of a multidimensional state variable, the RKF still chooses a scalar upper bound to clip the norm of multidimensional innovations. As a result, when the gross observation errors occur at a few variables, the norm of the innovations may not be influenced much by the few outliers and may not be clipped. In addition, once it selects a one-dimensional clipping height which is smaller than the norm, it should clip all the components of innovation no matter how large each component is.

Chapter 2 suggested a robust ensemble Kalman filter (REnKF) for the state estimation in a nonlinear system as a way of observation quality control used in data assimilation. While the REnKF retains the aforementioned features of the robust Kalman filter, it also introduces changes that select a vector of clipping heights to clip a vector of the innovations that are considered to be with outliers. We implemented and tested a performance of the REnKF on a 40-variable Lorenz model, concluding that bounding the innovations to reasonable values improves the performance of the filter in the presence of gross observation errors while causing only a modest loss of accuracy with clean data. Besides, Harlim and Hunt (2007) presented a non-Gaussian ensemble Kalman filter by using a distribution that decays more slowly

than a Gaussian distribution for background error distribution. Luo and Hoteit (2011) proposed a robust ensemble filtering scheme based on the H_∞ filtering theory, which is derived by minimizing the maximum of a predefined cost function. For robust Kalman filtering in a linear situation, Calvet et al. (2012) noticed that a impact function, which quantifies the sensitivity of the state distribution with respect to new data of a classical filter, is unbounded and proposed a filter with a bounded impact function. See Chapter 2 for more details and references about robust ensemble Kalman filtering schemes.

Although it is frequently essential that several state variables be estimated simultaneously, the RKF and REnKF were provided, and their application was investigated, to estimate one single state variable. So the main goal of the chapter is to apply the robust method to both linear and nonlinear dynamics of multiple state variables.

The rest of the chapter is organized as follows. Section 4.2 summarizes a classical (ensemble-based) Kalman filter for multiple variables, and provides a multivariate robust (ensemble-based) Kalman filter. Section 4.3 shows the simulation results in a linear model with the proposed multivariate robust Kalman filter, while Section 4.4 displays the results in a nonlinear model with the proposed multivariate robust ensemble-based Kalman filter.

4.2 Multivariate Robust Ensemble Kalman Filter

In this section, we inspect a multivariate ensemble Kalman filter and two different observational outlier models, and extend a robust ensemble Kalman filter described in Chapter 2 to a system of multiple state variables.

4.2.1 Multivariate ensemble-based Kalman filter

Suppose $\mathbf{x}_t = (\mathbf{x}_{1,t}, \mathbf{x}_{2,t}, \ldots, \mathbf{x}_{N,t}) \in \mathbb{R}^n$ is a finite-dimensional representation of N constituent state variables of the atmosphere at time t, where each n_i-dimensional constituent state $\mathbf{x}_{i,t}$ ($n = \sum_{i=1}^{N} n_i$). Let

$$\mathbf{x}_t = \mathcal{M}(\mathbf{x}_{t-1}) \tag{4.1}$$

be a model for the evolution of the multiple state variables between discrete times with a fixed interval. For the sake of simplicity, we assume that observations of the multiple state are taken at discrete times, for which the model solution is available, and that the functional relationship between the multivariate state, $\mathbf{x}_t$, and the vector of observations, $\mathbf{y}_t \in \mathbb{R}^p$, at time t is

$$\mathbf{y}_t = \mathbf{H}_t \mathbf{x}_t + \boldsymbol{\epsilon}_t, \tag{4.2}$$

where $\mathbf{y}_t = (\mathbf{y}_{1,t}, \ldots, \mathbf{y}_{N,t})$, $\mathbf{H}_t = \mathrm{diag}(\mathbf{H}_{1,t}, \ldots, \mathbf{H}_{N,t}) \in \mathbb{R}^{n \times p}$, and $\boldsymbol{\epsilon}_t = (\boldsymbol{\epsilon}_{1,t}, \ldots, \boldsymbol{\epsilon}_{N,t})$. Here, $\mathbf{y}_{i,t} \in \mathbb{R}^{p_i}$, $\mathbf{H}_{i,t} \in \mathbb{R}^{n_i \times p_i}$, and $\boldsymbol{\epsilon}_{i,t} \in \mathbb{R}^{n_i}$ are the vector of observations, the observation operation, and the vector of observation errors for the i-th state variable, respectively ($p = \sum_{i=1}^{N} p_i$). The relationship between the i-th state variable $\mathbf{x}_{i,t}$ and the corresponding vector of observation $\mathbf{y}_{i,t}$ is written as

$$\mathbf{y}_{i,t} = \mathbf{H}_{i,t} \mathbf{x}_{i,t} + \boldsymbol{\epsilon}_{i,t}. \tag{4.3}$$

Here, the observation error, $\boldsymbol{\epsilon}_{i,t}$ is assumed to be a zero-mean Gaussian process with a known covariance matrix, $\mathbf{R}_{i,t}$.

The Kalman filter provides an estimate of the multivariate state, $\mathbf{x}_t$, based on

the observations taken at the past and the present observation times and on the assumed knowledge of the dynamics. Dropping subscript t that denotes the time, let $\mathbf{x}^b$ be an n-dimensional background of the forecast, which is the best estimate of the multivariate state $\mathbf{x}$ before the assimilation of the observations at present time. We also let $\mathbf{P}^b$ be the $n \times n$-dimensional background-error covariance matrix for the multivariate state (i.e. $N \times N$ block matrix with (i, j)th block of dimension $n_i \times n_j$). In the Kalman filter algorithm, the multivariate analyzed state $\mathbf{x}^a$ is then given by

$$\mathbf{x}^a = \mathbf{x}^b + \mathbf{K}(\mathbf{y} - \mathbf{H}\mathbf{x}^b), \tag{4.4}$$

and the multivariate analysis-error covariance $\mathbf{P}^a$ is given by

$$\mathbf{P}^a = (\mathbf{I} - \mathbf{K}\mathbf{H})\mathbf{P}^b, \tag{4.5}$$

where the Kalman gain matrix, $\mathbf{K} \in \mathbb{R}^{n \times p}$, is

$$\mathbf{K} = \mathbf{P}^b\mathbf{H}^T(\mathbf{H}\mathbf{P}^b\mathbf{H}^T + \mathbf{R})^{-1}. \tag{4.6}$$

In the forecast step for a linear model, we obtain a complete solution to the background of the forecast and the background-error covariance matrix for the next time, which is computed directly from the model equation.

In an EnKF algorithm, the multivariate background-error covariance matrix, $\mathbf{P}^b \in \mathbb{R}^{n \times n}$, is approximated by the sample covariance matrix from a background ensemble of the forecasts. The multivariate background of the forecast is approximated by the mean of the background ensemble, $\bar{\mathbf{x}}_t^b$. The analysis step of the EnKF

then generates an analysis ensemble whose mean is

$$\bar{\mathbf{x}}^a = \bar{\mathbf{x}}^b + \mathbf{K}(\mathbf{y} - \mathbf{H}\bar{\mathbf{x}}^b). \tag{4.7}$$

The ensemble-based estimate of the multivariate analysis-error covariance matrix, $\mathbf{P}^a \in \mathbb{R}^{n\times n}$, defined by the sample covariance matrix for the ensemble, satisfies either (4.5) without the perturbed observations or

$$\mathbf{P}^a = (\mathbf{I} - \mathbf{KH})\mathbf{P}^b + O(M^{-1/2}) \tag{4.8}$$

with the perturbed observations. In our numerical experiments, we use the method of perturbed observations (Houtekamer and Mitchell, 1998; Burgers et al., 1998) to obtain the analysis ensemble. In this technique, $\mathbf{P}^a$ satisfies Eq. (4.8). The analysis process in the EnKF is completed by the forecast step, in which the model dynamics is applied to each member of the analysis ensemble in order to obtain the members of the background ensemble for the next observation time.

4.2.2 Observational outliers

Following the notations in Chapter 2, let

$$\mathbf{y}_t = \mathbf{H}_t\mathbf{x}_t + \boldsymbol{\xi}_t + \boldsymbol{\epsilon}_t, \tag{4.9}$$

be additive outlier model (AO), where some components of $\boldsymbol{\xi}_t \in \mathbb{R}^p$ are different from zero; and let

$$\boldsymbol{\epsilon}_t \sim (1-\alpha)N_p(\mathbf{0}, \mathbf{R}_t) + \alpha N_p(\mathbf{0}, k_t \cdot \mathbf{R}_t), \tag{4.10}$$

be the innovations outlier model (IO), where $0 < \alpha < 1$, $k_t = (k_{t1}, k_{t2}, \ldots, k_{tN})^T$, and some k_t's are bigger than 1. Here, N_p denotes the p-variate Gaussian distribution. In the innovations outlier model, some of observation errors come from a zero-mean Gaussian distribution having a larger variance than $\mathbf{R}_t$ with a contamination probability α.

4.2.3 A multivariate robust (ensemble-based) Kalman filter

The key idea of reducing detrimental effect of the outliers on the EnKF state estimate is to decrease the magnitude of those components of the innovation vector with unusually large absolute values (Roh et al., 2013). This can be done by defining an upper bound for the allowable absolute value of the innovations (i.e. clipping). When the magnitude of an innovation is larger than the prescribed upper bound, the magnitude of the innovation can be clipped at the upper bound. To be precise, the innovation δy is left unchanged if $-c < \delta y < c$ for some $c > 0$ and clipped at $-c$ if $\delta y < -c$ and at c if $\delta y > c$. This component-wise clipping of the innovation is called *Huberization*, and the tunable parameter, c, is called the *clipping height* (Roh et al., 2013).

A similar idea can be applied to a multivariate EnKF system and the clipping heights used to clip the multivariate true state may be determined simultaneously accounting for not only marginal-covariance structure of each state variable but also cross-covariance structure across different state variables. If multivariate true state variables are independent, clipping heights obtained from dealing with each state variable separately should be the same as those obtained from the method described below. A multivariate *Huberized analysis*, $\hat{\mathbf{x}}^a$, for the ensemble-based Kalman filter can be written as

$$\hat{\mathbf{x}}^a = \bar{\mathbf{x}}^b + \mathbf{K} G_{\mathbf{c}}(\mathbf{y} - \mathbf{H}\bar{\mathbf{x}}^b), \tag{4.11}$$

and for the Kalman filter,

$$\hat{\mathbf{x}}^a = \mathbf{x}^b + \mathbf{K}G_{\mathbf{c}}(\mathbf{y} - \mathbf{H}\mathbf{x}^b). \tag{4.12}$$

Here, for any $\mathbf{c} \in \mathbb{R}^p_+$ and $\mathbf{u} \in \mathbb{R}^p$, the *Huber* function, $G_{\mathbf{c}}(\mathbf{u})$, is defined as ($i = 1, \ldots, p$)

$$\{G_{\mathbf{c}}(\mathbf{u})\}_i = \begin{cases} u_i, & \text{if } |u_i| < c_i, \\ c_i, & \text{if } u_i \geq c_i, \\ -c_i, & \text{if } u_i \leq -c_i, \end{cases} \tag{4.13}$$

where c_i and u_i are the i-th elements of $\mathbf{c}$ and $\mathbf{u}$, respectively. The innovations are clipped component-wisely by the clipping height of the same index. When the Huberization achieves its goal of reducing the contamination of the prescribed distribution of the observation errors, the observation error covariance matrix, $\mathbf{R}$, provides a better representation of the observation error covariance. Hence, we do not modify any entries of $\mathbf{R}$ (Roh et al., 2013).

On the other hand, it is a common practice that suspect innovations are discarded from the data assimilation process for handling such innovations EnKF algorithms. Similarly to Roh et al. (2013), we compare a multivariate robust (ensemble-based) Kalman filter based on the Huberization with a traditional way of discarding, under the framework of multivariate (ensemble-based) Kalman filter which will be described in Sections 4.3 and 4.4.

4.2.4 Choosing the parameter $\mathbf{c}$

We now discuss the selection of the clipping height $\mathbf{c}$, which is a tuning parameter for handling gross observation errors. We take two criteria for the selection of clipping height, described in Chapter 2. One criterion is based on the relative efficiency, which

is defined by the ratio of the variance of the error in the estimates for two algorithms. The relative efficiency of robust EnKF and classical EnKF,

$$\delta = \frac{\mathrm{E}|\mathbf{x} - \bar{\mathbf{x}}^a|_{id}^2}{\mathrm{E}|\mathbf{x} - \hat{\mathbf{x}}^a|_{id}^2}, \tag{4.14}$$

falls into the interval $\delta \in (0, 1]$. Here, $|\cdot|$ denotes the Euclidean norm and the subscript id indicates that the norm is to be computed for clean, outlier-free, observations. For the robust Kalman filter in a linear situation, $\bar{\mathbf{x}}^a$ is substituted for $\mathbf{x}^a$. The classical (ensemble) Kalman filter with no clipping ($\mathbf{c} = \infty$) is identical to the Huberization with $\delta = 1$. On the other hand, the smaller δ is, the smaller the components of $\mathbf{c}$.

Another criterion is to select c_i such that

$$(1 - r)\mathrm{E}(|(\mathbf{y} - \mathbf{H}\bar{\mathbf{x}}^b)_i|_{id} - c_i)_+ = rc_i, \tag{4.15}$$

for a given radius $r \in (0, 1)$. Here, $(x)_+ = |x| \cdot \max\{x/|x|, 0\}$. The radius r is a proportion of the amount of clipping in the innovation. The clipping heights selected according to this criterion are the same for either type of clipping function, since this criterion does not depend on the clipping function. A smaller radius provides a larger clipping height, which clips fewer innovations.

As in Chapter 2, we use a Monte Carlo approach to compute the means for the denominator in Eqs. (4.14) and (4.15) by sampling from Gaussian distributions. Calculating the clipping height $\mathbf{c}$ at each time step is computationally burdensome, especially when the state variables are of high-dimension. Therefore, as in Chapter 2, we use $\lim_{t\to\infty} \mathbf{P}_t^b$, instead of letting $\mathbf{P}_t^b$ to be different at each time, for choosing one common vector of clipping height $\mathbf{c}$ across time steps. See Sections 4.3 and 4.4 for

more detailed examples.

4.3 Bivariate Linear Model

In this section, we illustrate the multivariate robust ensemble Kalman filter using a bivariate linear model.

For simplicity, we start with linear models for two state variables that Meinhold and Singpurwalla (1983) used:

$$x_{1,t} = x_{2,t} + e_{1,t}, \tag{4.16}$$

$$x_{2,t} = x_{2,t-1} + e_{2,t}, \tag{4.17}$$

where the model errors, $e_{1,t}$ and $e_{2,t}$, are uncorrelated white noises with mean zero and unit variance. The model equations can be written in vector notation as

$$\mathbf{x}_t = \mathbf{M}_t \mathbf{x}_{t-1} + \mathbf{e}_t = \begin{pmatrix} x_{2,t-1} + e_{1,t} + e_{2,t} \\ x_{2,t-1} + e_{2,t}, \end{pmatrix} \tag{4.18}$$

where $\mathbf{x}_t = \begin{pmatrix} x_{1,t} \\ x_{2,t} \end{pmatrix}$, $\mathbf{M}_t = \begin{pmatrix} 0 & 1 \\ 0 & 1 \end{pmatrix}$, and $\mathbf{e}_t = \begin{pmatrix} e_{1,t} + e_{2,t} \\ e_{2,t} \end{pmatrix}$ is the model error with mean zero and variance $\mathbf{Q_t} = \begin{pmatrix} 2 & 0 \\ 0 & 1 \end{pmatrix}$. We also observe only a state variable $x_{1,t}$, plus an observation error which is given by

$$y_t = x_{1,t} + \epsilon_t, \tag{4.19}$$

where the observation error, ϵ_t, is a zero-mean white noise with unit variance.

From the background of the model forecast, $\mathbf{x}_t^b$, and the background-error covari-

ance matrix, $\mathbf{P}_t^b$, the analysis, $\mathbf{x}_t^a$, and the analysis-error covariance matrix, $\mathbf{P}_t^a$, are directly obtained by Eqs. (4.4) and (4.5). In the forecast step, the background of the forecast and the background-error covariance matrix are obtained by

$$\mathbf{x}_{t+1}^b = \mathbf{M}_t \mathbf{x}_t^a, \tag{4.20}$$

$$\mathbf{P}_{t+1}^b = \mathbf{M}_t \mathbf{P}_t^a \mathbf{M}_t^T + \mathbf{Q}_t^a, \tag{4.21}$$

for the time step $t+1$.

As discussed in Section 4.2.4, we use the limit of $\mathbf{P}_t^b$, $\begin{pmatrix} 3 & 2 \\ 2 & 2 \end{pmatrix}$, to compute a common clipping height across time. Table 4.1 displays the clipping heights according to various efficiencies and radii, which clip the innovations related to one-dimensional observations.

Table 4.1: Clipping heights corresponding to efficiency and radius for the Huberization and discarding, respectively, in a bivariate linear model.

	efficiency			efficiency		
	0.9	0.8	0.7	0.01	0.05	0.1
Huberize	2.681	2.047	1.570	3.885	2.795	2.276
Discard	5.500	4.747	4.169	3.885	2.795	2.276

To examine the effect of the additive outliers on the Kalman filter, we assume that the additive outliers with $\xi_t = 10$ occur at times $t = 71$, 72, and 73 only at a variable x_1. Fig. 4.1 shows the boxplot of the bias of x_1 for the KF and two RKFs with various efficiencies. The efficiencies $\delta = 0.9$, 0.8, and 0.7 are used. At times $t = 71$ and 72, the Kalman filter state estimation deteriorates due to the additive outliers.

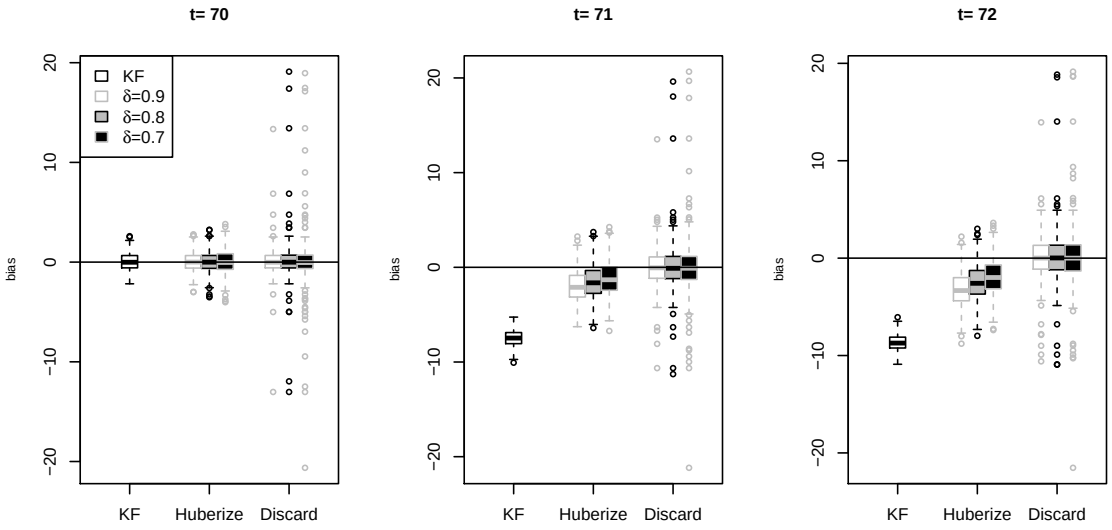

Figure 4.1: Bias vs efficiency for the KF and two RKFs for variable x_1 in a linear model. The additive outliers $\xi_t = 10$ occur at $t = 70, 71, 72$.

When the additive outliers occur in observation, bouding or discarding the gross observations reduces the estimation bias but increases the error variance. For any clipping, as the efficiency decreases, the error variance increases due to decreasing clipping height. At a fixed efficiency, when the outliers occur, the Huberization produces larger estimation bias but smaller error variance than the discarding. On the other hand, when the outliers do not occur, the estimation bias of both robust ensemble filters stay at zero at the expense of the error variance. In addition, the Huberization produces smaller error variance than the discarding.

Fig. 4.2 shows the boxplot of the bias for the KF and the two RKFs with various radii of the variable x_1. The radii $r = 0.01$, 0.05, and 0.1 are used. The figure shows that the Kalman filter state estimation is negatively influenced by the occuring additive outliers, and the two robust Kalman filters have the estimation

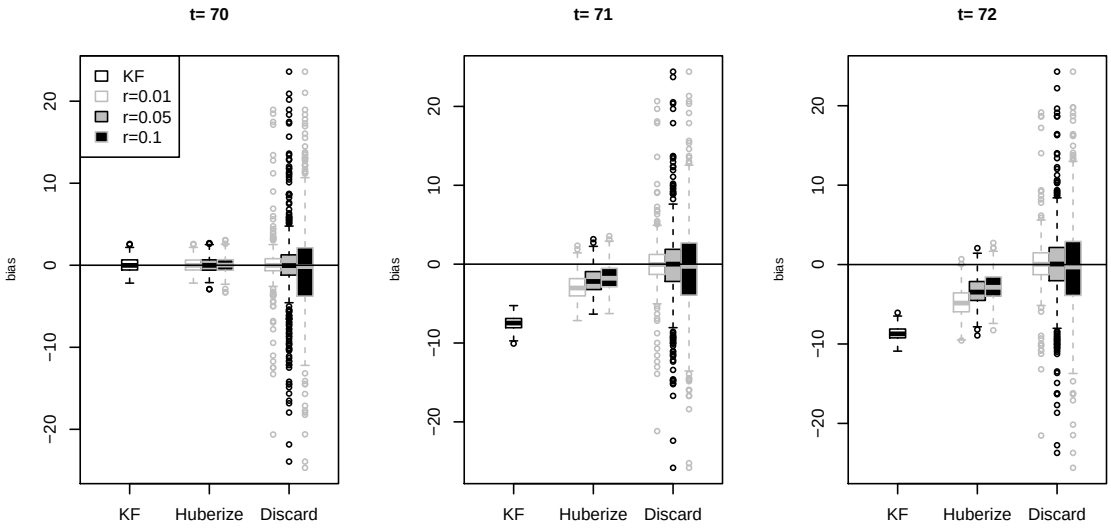

Figure 4.2: As in Fig. 4.1, but for bias vs radius.

bias closer to zero at the expense of increasing variation. As the radius increases, that is, the clipping height decreases, the Huberization reduces the bias slower than the discarding filter, while increasing the error variation slower than the discarding filter. Since a radius determines an identical clipping height regardless of type of clipping functions. It concludes that the Huberization appears to be less susceptible to outliers, compared to the discarding filter.

The left panel in Fig. 4.3 is a sample path out of 200 replications in Fig. 4.1, displaying the true states, the KF, and two RKFs with a efficiency $\delta = 0.8$. A huge jump of the traditional KF at times $t = 71$, 72, and 73 implies that there is a degradation in the state estimation due to occurring outliers. The right panel in Fig. 4.3 is a sample path out of 200 replications in Fig. 4.2, showing the true states, the KF, and two RKFs with a radius $r = 0.05$. This panel also shows that the state estimation of the traditional Kalman filter degenerates in the presence of outliers.

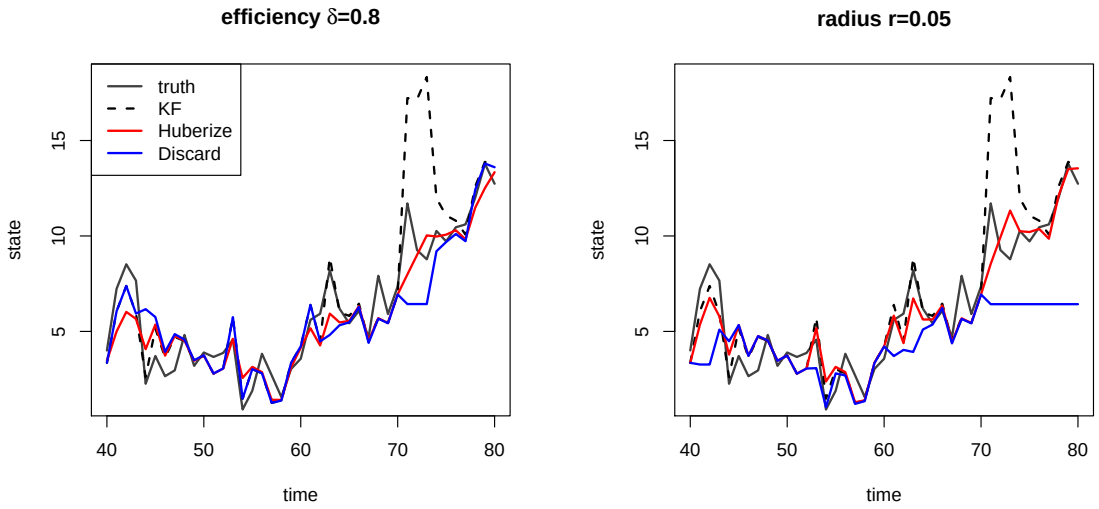

Figure 4.3: Plot of the true states x_1, the traditional KF, and the two RKFs with a (left) efficiency $\delta = 0.8$ and a (right) radius 0.05, respectively, in a bivariate linear system. The additive outliers $\xi_t = 10$ occur at $t = 71, 72, 73$.

In addition, for a radius $r = 0.05$, getting rid of extremely large observations has a detrimental effect on the accuracy of the state estimation, whereas the Huberization reduces the jump safely.

For the innovations outliers, we assume the innovations outliers with $k_t = 20$ and $\alpha = 0.2$ occur at times $t = 71$ and 72 only at a variable x_1. Fig. 4.4 shows the bias of the KF and two RKFs with various efficiencies. We use the efficiencies $\delta = 0.9$, 0.8, and 0.7. The estimation bias of the two robust filters stays at zero, since the mean of innovations error is set to be zero. The occuring innovations outliers, however, force the classical KF to have a large error variances but to keep a zero mean. For time $t = 70$, discarding such outliers with smaller efficiency results in a faster increase of the error variance compared to the Huberization. For times $t = 71$ and 72, as the efficiency decreases, the error variance decreases for the Huberization

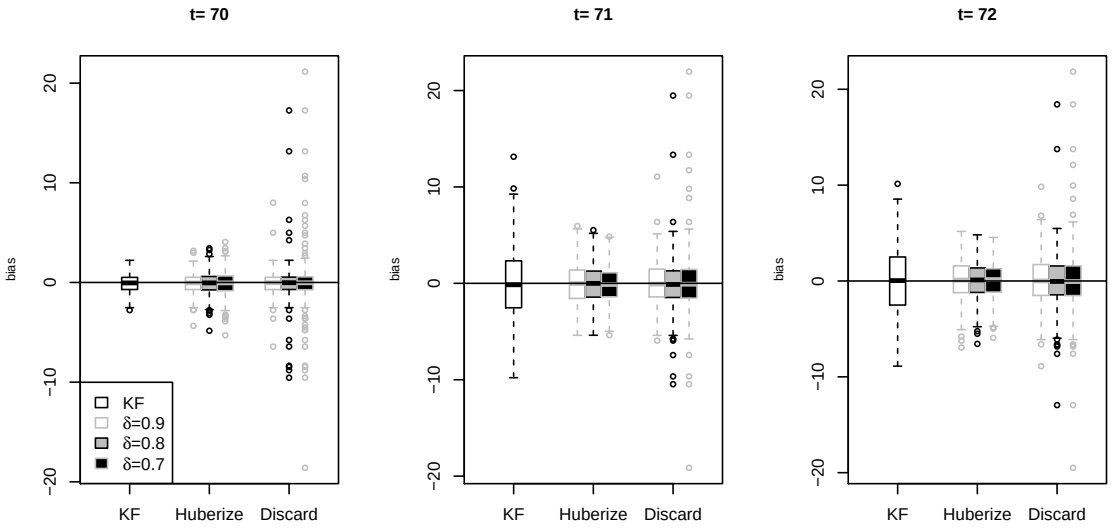

Figure 4.4: As in Fig. 4.1, but for the innovations outliers with $k_t = 20$ and $\alpha = 0.2$.

but increases for the discarding. It is concluded that at a fixed efficiency, dropping the gross observations tends to experience a faster increase of the error variance than the Huberization.

Fig. 4.5 presents the bias of the KF and the two RKFs with various radii. We use the radii $r = 0.01$, 0.05, and 0.1. With these radii, the Huberization outperforms the discarding, while both types of clipping expend the increasing error variance. The figure also shows that the error variance of discarding outliers is more sensitive to the radius, and is likely to be influenced by the small change in the radius than the Huberization.

4.4 Bivariate Nonlinear Model

In this section, we illustrate the multivariate robust ensemble Kalman filter using a bivariate Lorenz model.

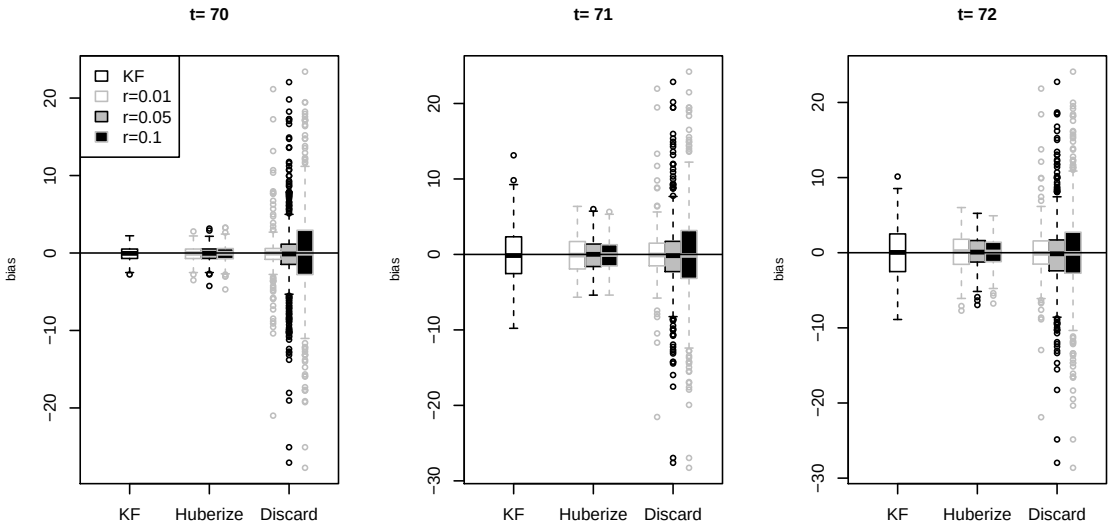

Figure 4.5: As in Fig. 4.4, but for bias vs radius.

4.4.1 The bivariate Lorenz model

We now consider a coupled system for two state variables introduced in Lorenz (1995). There are K variables, X_k, and JK variables, $Y_{j,k}$ for $j = 1, \ldots, J$ and $k = 1, \ldots, K$, equally spaced on a latitude circle. The governing equations are

$$\frac{dX_k}{dt} = -X_{k-1}(X_{k-2} - X_{k+1}) - X_k - (hc/b)\sum_{j=1}^{J} Y_{j,k} + F + \frac{dW_k}{dt}, \tag{4.22}$$

$$\frac{dY_{j,k}}{dt} = -cbY_{j+1,k}(Y_{j+2,k} - Y_{j-1,k}) - cY_{j,k} + (hc/b)X_k + \frac{dZ_{j,k}}{dt}, \tag{4.23}$$

where the system errors dW_k and $dZ_{j,k}$ are uncorrelated white noise with mean zero and variance 0.005. We let X_{k-K} and X_{k+K} equal to X_K, and let $Y_{j,k-K}$ and $Y_{j,k+K}$ equal to $Y_{j,k}$, while $Y_{j-J,k} = Y_{j,k-1}$ and $Y_{j+J,k} = Y_{j,k+1}$. Here, X_k represents the values of some quantity in K sectors of a latitude circle, while $Y_{j,k}$ represents the

values of some other quantity in JK sectors.

We let $K = 36$ and $J = 10$ so that there are 10 small sectors, each one degree of longitude in length in one large sector, and we use the same parameters as in Lorenz (1995); $c = 3$ and $b = 3$, implying that the convective-scale state $Y_{j,k}$ tends to fluctuate 3 times as rapidly as the state X_k, while its amplitude is 1/3 as large. We use a coupling coefficient $h = 1$, a forcing term $F = 10$, and a fourth-order Runge-Kutta time integration scheme with a time step of 0.005 non-dimensional units. Fig 4.6 displays a longitudinal profile of the two state variables X and Y, determined with these parameters.

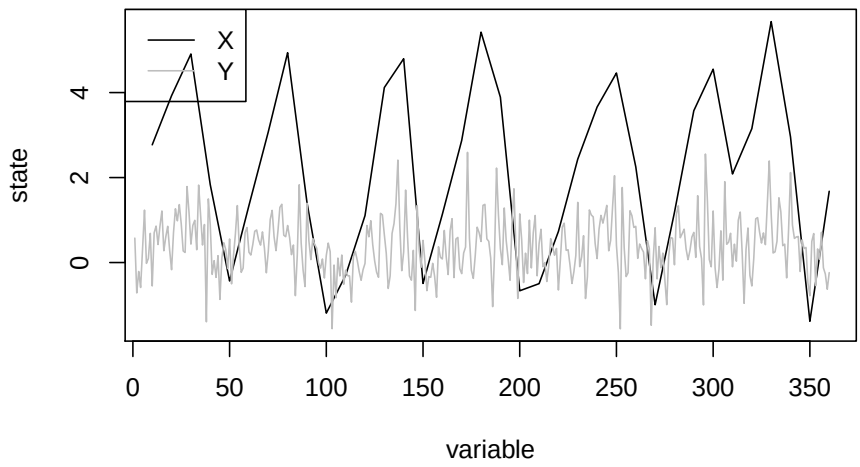

Figure 4.6: Longitudinal profiles of X and Y, as determined by Eqs. (4.22) and (4.23) with $b = 3$, $c = 3$, and $h = 1$.

4.4.2 Experimental results

The experiments were conducted using the EnKF and REnKF with perturbed observations. We use twenty-member ensembles with an ensemble inflation factor of 2, and at every time step we assimilate the observations having uncorrelated observation errors which is a zero-mean Gaussian process with a variance of 0.005. We repeat this simulation 200 times for boxplots we will show. To compute a common vector of clipping height over time, an average of $\mathbf{P}_t^b$ between $t = 1901 - 2000$ from 5000-member ensembles is used as a limit of $\mathbf{P}_t^b$. In computing $\mathbf{P}_t^b$, we run the model forward and assimilate observations.

As described in Chapter 3, to reduce the sampling errors in multivariate covariance matrix consisting of marginal- and cross-covariance matrices, we may use a localization method. Unlike a univariate case, extra care is necessary to implement the localization methods on the cross-covariance matrix so that the localized multivariate covariance matrix could maintain its positive-definiteness. To ensure that the localized bivariate covariance for the Lorenz model is positive-definite, we use the Gaspari-Cohn function with a localization constant of 40 for marginal-covariance and cross-covariance matrices, respectively, and then multiply the cross-covariance matrices by 0.5.

Fig. 4.7 displays three common vectors of clipping heights, $\mathbf{c}$, corresponding to a efficiency $\delta = 0.999$ for the Huberization and the discarding, respectively, and corresponding to a radius $r = 0.01$. The first 36 variables in black are for the variable X, and the other variables in gray are for the variable Y. A vector of clipping heights determined by a radius is used for both of the Huberization and the discarding, since the radius criterion does not involve the clipping function. This figure illustrates that at a fixed efficiency, the corresponding clipping heights for the Huberization

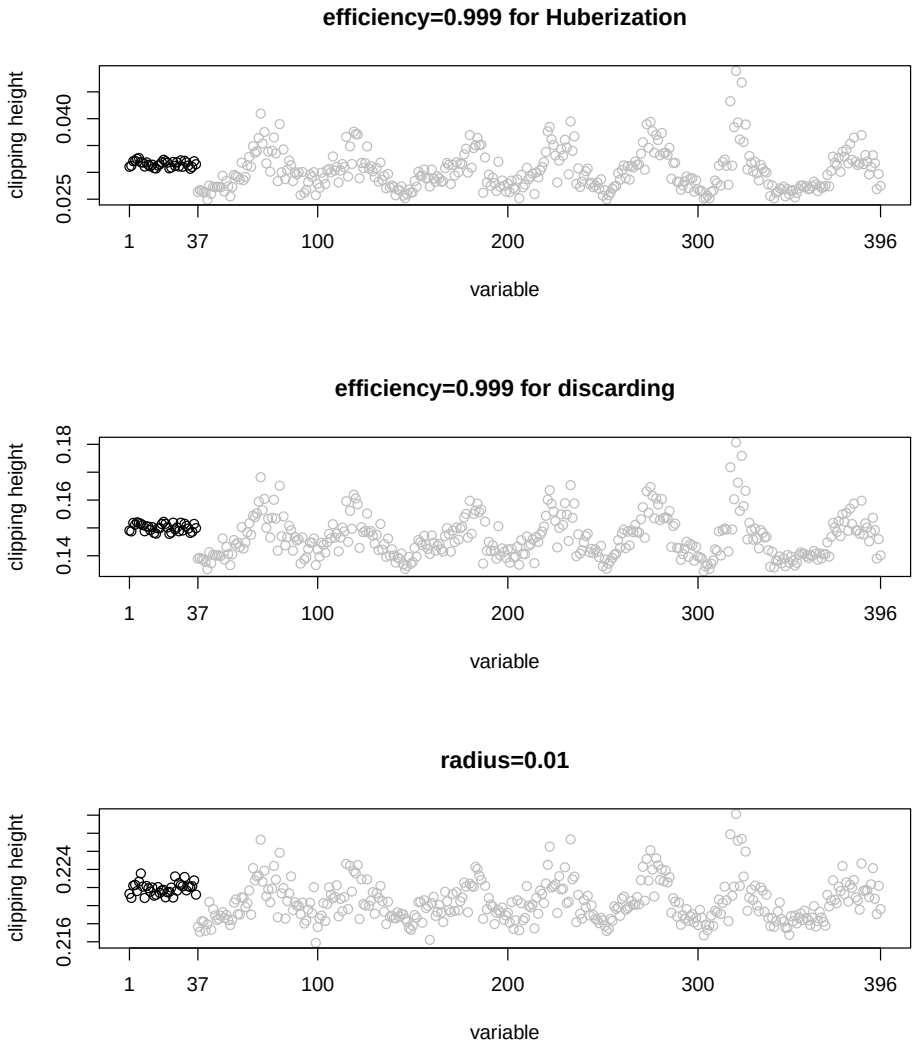

Figure 4.7: Clipping heights according to efficiency $\delta = 0.999$ for (top) Huberization and (middle) discarding, respectively, and (bottom) radius $r = 0.01$ for the bivariate Lorenz model. Clipping heights for X and Y are black and gray, respectively.

are smaller than those for the discarding. This is because larger values of clipping heights discard a smaller number of observations, and because the relative efficiency of bounding outliers to a proper clipping valuets should be larger than that of making outliers to zero.

To inspect the effect of additive outliers, we assume that the additive outliers with $\xi_t = 5$ occur at variables X_{32} and X_{33} at times $t = 1512$ and 1513. Fig. 4.8 displays the bias of EnKF and the two REnKFs with various efficiencies at variables X_{33}. We use the efficiencies $\delta = 0.99999$, 0.9999, and 0.999. The figure shows

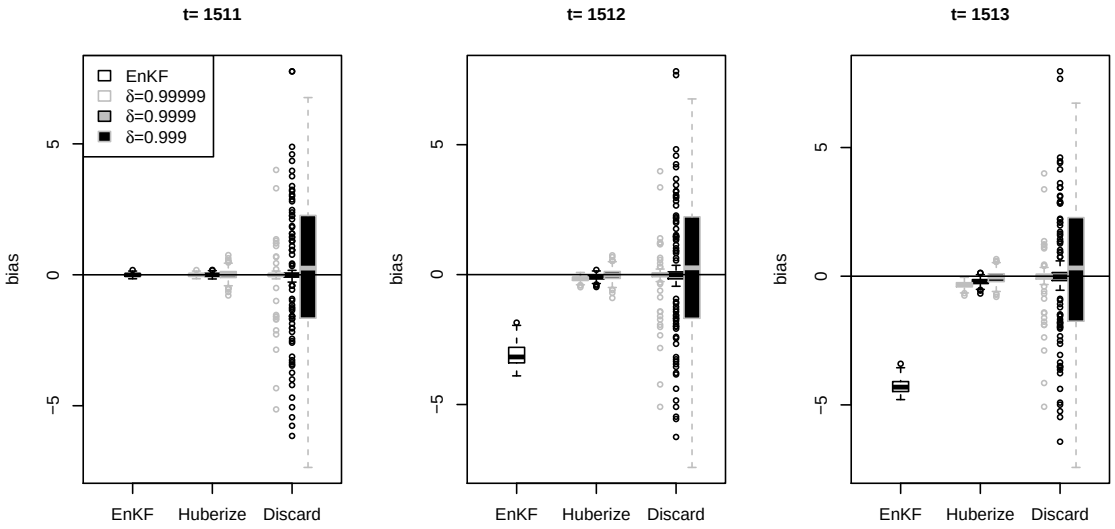

Figure 4.8: Bias vs efficiency of the EnKF and two REnKFs for variable X_{33} of the bivariate Lorenz model. The additive outliers with $\xi_t = 5$ occur at times $t = 1512$ and 1513.

that the additive outliers compel the classical EnKF to have a large estimation bias. The additive outliers at time $t = 1512$ degrade the state estimation, and still

have a negative impact on the state estimation for the next time step $t = 1513$. The Huberization reduces both the estimation bias and the error variance, while discarding suspect observations reduces the estimation bias at the expense of the increasing error variance.

Fig. 4.9 shows the bias of EnKF and the two REnKFs with various radii at variables X_{33}. We use the radii $r = 0.00001$, 0.001, and 0.01, and the results from using

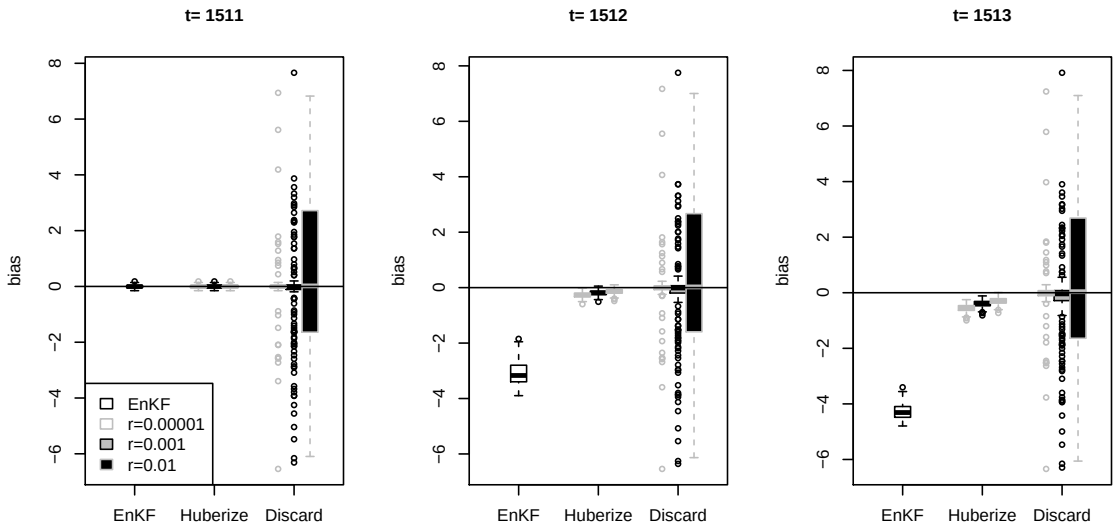

Figure 4.9: As in Fig. 4.8, but for bias vs radius.

these radii are similar to those from using the efficiencies above. The Huberization reduces both the bias and the variation, whereas the discarding filter immensely increases the error variance.

The left panel of Fig. 4.10 is a sample path out of 200 replications, displaying a trajectory of the true states, the EnKF, and the two REnKFs with a efficiency

$\delta = 0.999$ occurring at variable X_{33}. The right panel of Fig. 4.10 is a sample path

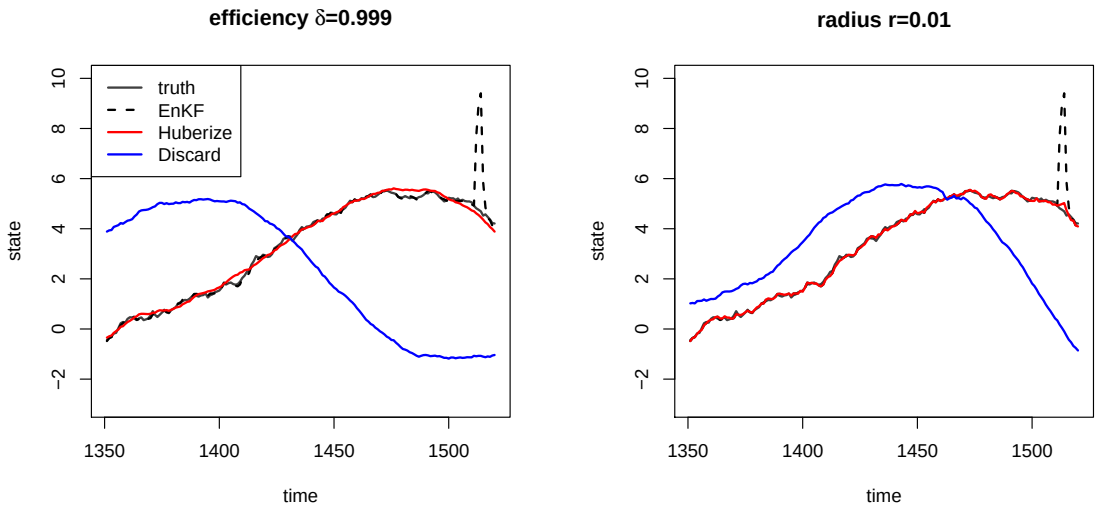

Figure 4.10: The true states, EnKF, and two REnKFs with a (left) efficiency $\delta = 0.999$ and a (top) radius $r = 0.01$, respectively, for variable X_{33} of the bivariate Lorenz model. The additive outliers with $\xi_t = 5$ occur at times $t = 1512, 1513, 1514$.

out of 200 replications, showing the true states, the EnKF, and the two REnKFs with a radius $r = 0.01$ at variable X_{33}. From both panels, discarding spurious observations results in an inaccurate state estimation, whereas Huberizing them is more accurate regardless of the presence and absence of outliers.

To investigate the influence of innovations outliers, we assume that the innovations outliers with $k_t = 100$ and a contamination probability of $\alpha = 0.2$ at variables X_{32} and X_{33} at times $t = 1512$ and 1513. In Fig. 4.11, we present the bias of the EnKF and the two REnKFs with various efficiencies. We use the efficiencies $\delta = 0.99999$, 0.9999, and 0.999. The innovations outlier produces a large error variation of the classical EnKF. On the other hand, the state estimation of the Huber-

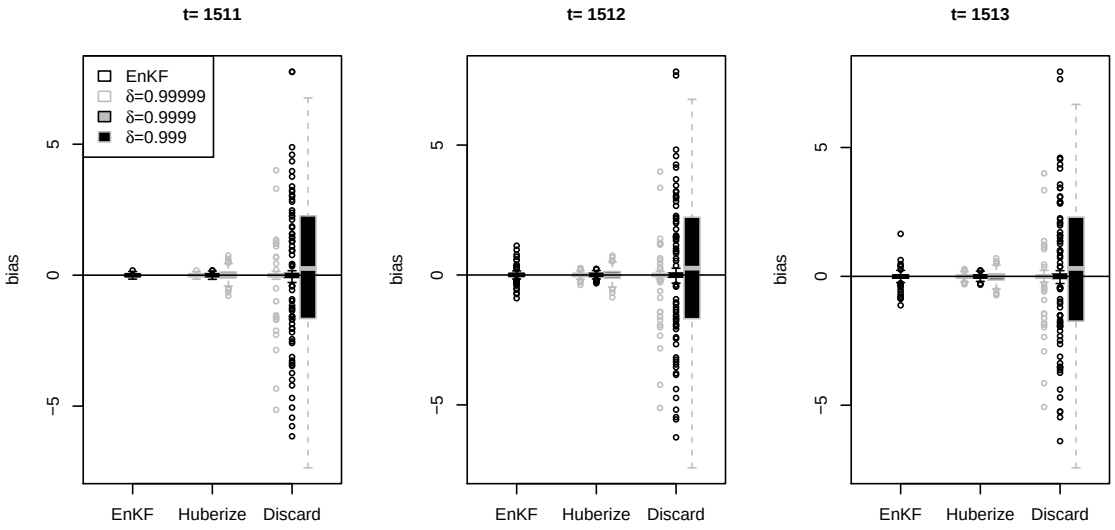

Figure 4.11: As in Fig. 4.8, but for innovations outliers with $k_t = 100$ with a probability of contamination $\alpha = 0.2$.

ization is more accurate and is less likely to experience the increasing error variance. The error variance from dropping outliers is larger then that from Huberizing outliers, and is larger even than the classical EnKF. From the middle panel of Fig. 4.11, the Huberization reduces the error variariance to a point but then increases it again when the clipping height reaches a small value enough to truncate a innovation from an outlier-free observation.

Fig. 4.12 illustrates the bias of the EnKF and the two REnKFs with various radii. The radii $r = 0.00001$, 0.001, and 0.01 are used. As the radius increases, the error variance decreases for the Huberization, while it increases for the discarding. From $r = 0.001$ to $r = 0.1$, there is a sudden change in the interquantile range of the error variance for the discarding, implying that the discarding is more sensitive to the small change in the value of radius than the Huberization.

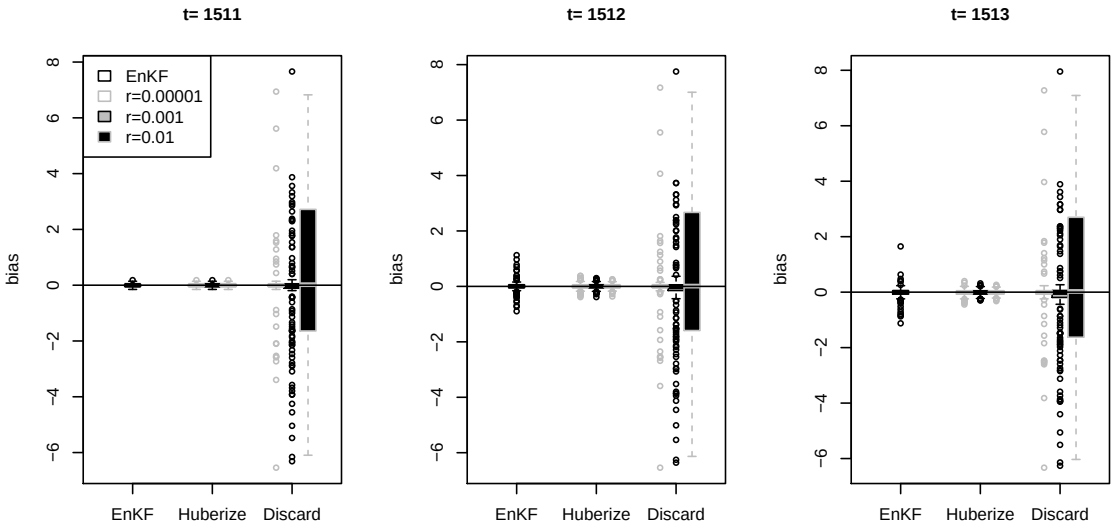

Figure 4.12: As in Fig. 4.11, but for bias vs radius.

5. SUMMARY

In this dissertation, first, we proposed a robust ensemble Kalman filter for the robust estimation of the state of a spatio-temporal dynamical system in the presence of observational outliers. We also proposed two criteria of effiiciency and radius to select clipping heights. We compared the results of the robust ensemble Kalman filter with those from the classical ensemble Kalman filter, and also compared the robust ensemble Kalman filter based on the Huberization filter, which pulls the outliers back to $\mathbf{c}$ or $-\mathbf{c}$, and another ensemble Kalman filter, which discards outliers. As we applied the robust ensemble Kalman filter to a one-dimensional linear system and a multidimensional nonlinear system, we found that compared to the conventional EnKF, the robust ensemble Kalman filter reduced the bias in the state estimates at the expense of increasing the error variance. The increase of the error variance differed depending on the filtering method. The Huberization was found to perform better than discarding suspect observations in the examples given in the dissertation. It may be because the model we used gives the true state. The robust ensemble Kalman filter is efficient with simple models, and we plan to test it in realistic ocean and atmospheric systems.

Second, we introduced multivariate localization methods for the EnKF algorithms in the system of two or more state variables. The proposed method localizes both marginal- and cross-covariances by using a valid localization function and adjusts the cross-covariances so that the multivariate ensemble covariance could succeed in achieving the positive-definiteness. We used a bivariate Lorenz model, where two state variables are coupled to each other, in order to test the performance of the proposed multivariate localization method. We compared two different observation

scenarios and compared the Gaspari-Cohn function and the Askey function, which are compactly supported correlation functions. Localizing and adjusting both marginal- and the cross-covariances improve the performance of ensemble Kalman filter in terms of the root mean square error, especially when a small portion of a dominant variable is observed.

Lastly, we investigated the robust ensemble Kalman filter technique in both linear and nonlinear dynamical systems of multiple state variables. We tested the robust (ensemble) Kalman filter with the help of a bivariate linear system and a bivariate nonlinear system. Using the Huberization method which bounds the observation outliers, the negative effects of outliers on the state estimates can be greatly reduced. It was found to perform better than the filter which discards them in the examples given in the dissertation.

REFERENCES

Anderson, E. and Järvinen, H. (1999), "Variational quality control," *Quarterly Journal of the Royal Meteorological Society*, 125, 697–722.

Anderson, J. and Lei, L. (2013), "Empirical localization of observation impact in ensemble Kalman filters," *Monthly Weather Review*, 142, 739–754.

Anderson, J. L. (2001), "An ensemble adjustment filter for data assimilation," *Monthly Weather Review*, 129, 2884–2903.

— (2007), "Exploring the need for localization in ensemble data assimilation using a hierarchical ensemble filter," *Physica D*, 230, 99–111.

Askey, R. (1973), "Radial characteristic functions," technical report no. 1262, Mathematical Research Center, University of Wisconsin-Madison, Madison.

Bevilacqua, M., Daryl, J. D., Porcu, E., and Schlather, M. (2013), "Classes of compactly supported correlation functions for multivariate random fields," technical report, Universidad Federico Santa Maria.

Bhatia, R. (1997), *Matrix analysis*, New York: Springer.

Birmiwal, K. and Papantoni-Kazakos, P. (1994), "Outlier resistant prediction for stationary processes," *Statistical Decision*, 12, 395–427.

Birmiwal, K. and Shen, J. (1993), "Optimal robust filtering," *Statistical Decision*, 11, 101–119.

Bishop, C. H. and Hodyss, D. (2007), "Flow adaptive moderation of spurious ensemble correlations and its use in ensemble based data assimilation," *Quarterly Journal of the Royal Meteorological Society*, 133, 2029–2044.

— (2009a), "Ensemble covariances adaptively localized with ECO-RAP. Part 1: Tests on simple error models," *Tellus*, 61A, 84–96.

— (2009b), "Ensemble covariances adaptively localized with ECO-RAP. Part 2: A strategy for the atmosphere," *Tellus*, 61A, 97–111.

Buehner, M. and Charron, M. (2007), "Spectral and spatial localization of background-error correlations for data assimilation," *Quarterly Journal of the Royal Meteorological Society*, 133, 615–630.

Burgers, G., van Leeuwen, P. J., and Evensen, G. (1998), "Analysis scheme in the ensemble Kalman filter," *Monthly Weather Review*, 126, 1719–1724.

Calvet, L. E., Czellar, V., and Ronchetti, E. (2012), "Robust filtering," http://ssrn.com/abstract=2123477.

Campbell, W. F., Bishop, C. H., and Hodyss, D. (2010), "Vertical covariance localization for satellite radiances in ensemble Kalman filters," *Monthly Weather Review*, 138, 282–290.

Daley, R. (1991), *Atmospheric Data Analysis*, Cambridge Atmospheric and Space Science Series, Cambridge University Press.

Du, J. and Ma, C. (2013), "Vector random fields with compactly supported covariance matrix functions," *Journal of Statistical Planning and Inference*, 143, 457–467.

Ershov, A. A. and Liptser, R. S. (1978), "Robust Kalman filter in discrete time," *Automatic and Remote Control*, 39, 359–367.

Evensen, G. (1994), "Sequential data assimilation with a nonlinear quasi-geostrophic model using Monte Carlo methods to forecast error statistics," *Journal of Geological Research*, 99, 10143–10162.

Fahrmeir, L. and Kaufmann, H. (1991), "On Kalman filtering, posterior mode estimation and Fisher scoring in dynamic exponential family regression," *Metrika*, 38, 37–60.

Fahrmeir, L. and Kunstler, R. (1999), "Penalized likelihood smoothing in robust

state space models," *Metrika*, 49, 173–191.

Fox, A. J. (1972), "Outliers in time series," *Journal of the Royal Statistical Society, Series B*, 34, 350–363.

Gaspari, G. and Cohn, S. E. (1999), "Construction of correlation functions in two and three dimensions," *Quarterly Journal of the Royal Meteorological Society*, 125, 723–757.

Genton, M. G. (2003), "Breakdown-point for spatially and temporally correlated observations," in *Developments in Robust Statistics, International Conference on Robust Statistics 2001*, eds. Dutter, R., Filzmoser, P., Gather, U., and Rousseeuw, P. J., Springer, Heidelberg, pp. 148–159.

Genton, M. G. and Lucas, A. (2003), "Comprehensive definitions of breakdown-points for independent and dependent observations," *Journal of the Royal Statistical Society, Series B*, 65, 81–94.

— (2005), "discussion of "Breakdown and groups" by L. Davies and U. Gather," *Annals of Statistics*, 33, 988–993.

Gneiting, T. (1999), "Correlation functions for atmospheric data analysis," *Quarterly Journal of the Royal Meteorological Society*, 125, 24492464.

— (2002), "Compactly supported correlation functions," *Journal of Multivariate Analysis*, 83, 493–508.

Hamill, T. M., Whitaker, J. S., and Snyder, C. (2001), "Distance-Dependent Filtering of Background Error Covariance Estimates in an Ensemble Kalman Filter," *Monthly Weather Review*, 129, 2776–2790.

Hampel, F. R. (1986), "Contributions to the theory of robust estimation," Ph.D. thesis, University of California, Berkely.

Harlim, J. and Hunt, B. R. (2007), "A non-Gaussian ensemble filter for assimilating infrequent noisy observations," *Tellus A*, 59, 225–237.

Houtekamer, P. L. and Mitchell, H. L. (1998), "Data assimilation using an ensemble Kalman filter technique," *Monthly Weather Review*, 126, 796–811.

— (2001), "A Sequential Ensemble Kalman Filter for Atmospheric Data Assimilation," *Monthly Weather Review*, 129, 123–137.

Huber, P. J. (1981), *Robust Statistics*, New York: Wiley.

Hunt, B. R., Kostelich, E. J., and Szunyogh, I. (2007), "Efficient data assimilation for spatiotemporal chaos: A local ensemble transform Kalman filter," *Physica D*, 230, 112–126.

Ingleby, N. B. and Lorenc, A. C. (1993), "Bayesian quality control using multivariate normal distributions," *Quarterly Journal of the Royal Meteorological Society*, 119, 1195–1225.

Jun, M., Szunyogh, I., Genton, M. G., Zhang, F., and Bishop, C. H. (2011), "A Statistical Investigation of the Sensitivity of Ensemble-Based Kalman Filters to Covariance Filtering," *Monthly Weather Review*, 139, 3036–3051.

Kalman, R. E. (1960), "A new approach to linear filtering and prediction problems," *Journal of Basic Engineering*, 82, 34–45.

Kalman, R. E. and Bucy, R. S. (1961), "New results in linear filtering and prediction theory," *Journal of Basic Engineering*, 95–108.

Kassam, S. A. and Poor, H. V. (1985), "Robust techniques for signal processing: a survey," *Proc. IEEE*, 73, 433–481.

Kleiber, W. and Porcu, E. (2013), "Nonstationary matrix covariances: Compact support, long range dependence and adapted spectra," *technical report*.

Lei, L. and Anderson, J. (2014), "Comparison of empirical localization techniques for serial ensemble Kalman filters in a simple atmospheric general circulation model," *Monthly Weather Review*, 141, 4140–4153.

Lorenz, E. N. (1995), "Predictability-A problem partly solved," Vol. 1. ECMWF,

Reading, Berkshire, UK.

Lorenz, E. N. and Emanuel, K. A. (1998), "Optimal sites for supplementary weather observations: Simulation with a small model," *J. Atmos. Sci.*, 55, 399–414.

Luo, X. and Hoteit, I. (2011), "Robust ensemble filtering and its relation to covariance inflation in the ensemble Kalman filter," *Monthly Weather Review*, 139, 3938–3953.

Maronna, A., Martin, R. D., and Yohai, V. J. (2006), *Robust Statistics: Theory and Methods*, Chichester, England: Wiley.

Martin, R. D. and Raftery, A. E. (1987), "Robustness, computation and non Euclidean models," *Journal of the American Statistical Association*, 82, 1044–1050.

Meinhold, R. J. and Singpurwalla, N. D. (1983), "Understanding the Kalman filter," *American Statistician*, 37, 123–127.

— (1989), "Robustification of Kalman filter models," *Journal of the American Statistical Association*, 84, 479–486.

Naveau, P., Genton, M. G., and Shen, X. (2005), "A skewed Kalman filter," *Journal of Multivariate Analysis*, 95, 382–400.

Ott, E., Hunt, B. R., Szunyogh, I., Zimin, A. V., Kostelich, E. J., Corazza, M., Kalnay, E., Patil, D. J., and Yorke, J. A. (2004), "A local ensemble Kalman filter for atmospheric data assimilation," *Tellus*, 56A, 415–428.

Porcu, E., Daley, D. J., Buhmann, M., and Bevilacqua, M. (2012), "Radial basis functions with compact support for multivariate geostatistics," *Stochastic Environmental Research and Risk Assessment*, 27, 909–922.

Roh, S., Genton, M. G., Jun, M., Szunyogh, I., and Hoteit, I. (2013), "Observation quality control with a robust ensemble Kalman filter," *Monthly Weather Review*, 141, 4414–4428.

Ruckdeschel, P. (2010), "Optimally robust Kalman filtering," *Berichte des Fraun-*

hofer ITWM, 185, 1–53.

Schick, I. C. and Mitter, S. K. (1994), "Robust recursive estimation in the presence of heavy-tailed observation noise," *Annals of Statistics*, 22, 1045–1080.

Schlee, F. H., Standish, C. J., and Toda, N. F. (1967), "Divergence in the Kalman filter," *The American Institute of Aeronautics and Astronautics*, 5, 1114–1120.

Stockinger, N. and Dutter, R. (1987), "Robust time series analysis: A survey," *Kybernetika*, 23, 3–88.

Szunyogh, I., Kostelich, E. J., Gyarmati, G., Kalnay, E., Hunt, B. R., Ott, E., Satterfield, E., and Yorke, J. A. (2008), "A local ensemble transform Kalman filter data assimilation system for the NCEP global model," *Tellus*, 60A, 113–130.

Tavolato, C. and Isaksen, L. (2010), "Huber norm quality control in the IFS," *ECMWF Newsletter*, 122, 27–31.

Tukey, J. W. (1970), *Exploratory Data Analysis (Limited Preliminary Edition)*, vol. 1, Reading, MA: Addison-Wesley, Chapter 5.

Wendland (1995), "Piecewise polynomial, positive denite and compactly supported radial functions of minimal degree," *Advances in Computational Mathematics*, 4, 389–396.

West, M. (1981), "Robust sequential approximate Bayesian estimation," *Journal of the Royal Statistical Society, Series B*, 43, 157–166.

— (1983), "Generalized linear models: Scale parameters, outlier accommodation and prior distributions," *Bayesian Statistics 2*, 1, 531–558.

— (1984), "Outlier models and prior distributions in Bayesian linear regression," *Journal of the Royal Statistical Society, Series B*, 46, 431–439.

Whitaker, J. S. and Hamill, T. M. (2002), "Ensemble data assimilation without perturbed observations," *Monthly Weather Review*, 130, 1913–1924.

Zhang, H. and Du, J. (2008), "Covariance Tapering in Spatial Statistics," Eds. J.

Mateu and E. Porcu, Spain: Graficas Casta n, s.l.